

Mini Review

Open Access



# Hydrogen and organic synthesis from wastewater with nano photocatalysts: a synergy

Muhammad Khalid Hussain<sup>1</sup>, Ruhan Liu<sup>1</sup>, Muhammad Tanveer<sup>2</sup>, N. R. Khalid<sup>3</sup>, Zonyou Yin<sup>1\*</sup>

<sup>1</sup>Research School of Chemistry, Australian National University, Canberra ACT 2601, Australia.

<sup>2</sup>Department of Physics, Faculty of Science, University of Gujrat, Gujrat 50700, Pakistan.

<sup>3</sup>Department of Physics, Institute of Physics and Materials Science, University of Okara, Okara 56300, Pakistan.

\*Correspondence to: Prof. Zonyou Yin, Research School of Chemistry, Australian National University, Building 137, Sullivans Creek Road, Canberra ACT 2601, Australia. E-mail: zongyou.yin@anu.edu.au

**How to cite this article:** Hussain, M. K.; Liu, R.; Tanveer, M.; Khalid, N. R.; Yin, Z. Hydrogen and organic synthesis from wastewater with nano photocatalysts: a synergy. *Chem. Synth.* **2025**, *5*, 40. <https://dx.doi.org/10.20517/cs.2024.99>

**Received:** 15 Aug 2024 **First Decision:** 15 Oct 2024 **Revised:** 22 Nov 2024 **Accepted:** 23 Dec 2024 **Published:** 10 Apr 2025

**Academic Editors:** Xiang-Dong Yao, Aicheng Chen **Copy Editor:** Pei-Yun Wang **Production Editor:** Pei-Yun Wang

## Abstract

Nano-photocatalysts exhibit significant potential for diverse applications, including the degradation of organic pollutants, hydrogen generation through water splitting, organic synthesis, and photoelectrochemical conversion. Recently, there has been growing interest in the efficient utilization of wastewater and liquid organic waste as resources for organic synthesis and hydrogen production. This approach offers a promising solution to both energy and environmental challenges by enabling hydrogen and organic synthesis from wastewater using nanophotocatalysts. Dual-functional nanophotocatalysts demonstrated significant potential for efficient catalysis processes. This review provides a comprehensive analysis of various nano-photocatalysts, their synthesis processes, and the underlying photocatalytic mechanisms that drive the synergistic effects, leading to enhanced efficiency. Furthermore, the resulting photocatalytic products and their implications are discussed in detail. Key challenges associated with this emerging technology are identified, along with future research directions to advance its development. By highlighting recent advancements in the use of nano-photocatalysts for hydrogen generation and organic compound synthesis from wastewater and liquid organic waste, this review serves as a valuable resource to guide ongoing and future research efforts in this field.

**Keywords:** Nano-photocatalysts, organic wastewater, hydrogen production, organic synthesis, synergistic effects



© The Author(s) 2025. **Open Access** This article is licensed under a Creative Commons Attribution 4.0 International License (<https://creativecommons.org/licenses/by/4.0/>), which permits unrestricted use, sharing, adaptation, distribution and reproduction in any medium or format, for any purpose, even commercially, as long as you give appropriate credit to the original author(s) and the source, provide a link to the Creative Commons license, and indicate if changes were made.



## INTRODUCTION

In recent decades, global awareness of the escalating energy demands and environmental challenges associated with fossil fuel consumption has increased significantly. Gong *et al.* reported that these growing concerns have fueled increased global awareness over the past few decades. Currently, the global energy supply primarily relies on fossil fuels, including coal, oil, and natural gas. However, these fossil fuel reserves are rapidly depleting, and global energy demand is projected to double by 2025 because of rapid industrialization and population growth<sup>[1,2]</sup>. Furthermore, George *et al.* reported that fossil fuel consumption generates toxic emissions, posing significant environmental threats. To address these challenges, significant advancements in materials science and engineering have been made to develop efficient energy-conversion technologies and environmental preservation strategies<sup>[3,4]</sup>. Bard *et al.* reported that among the various methods investigated, semiconductor-based photocatalysis has emerged as a promising technology with a significant interdisciplinary interest in environmentally friendly energy solutions. This technology has significant potential for harnessing clean and sustainable solar energy for a wide range of energy and environmental applications<sup>[5-15]</sup>. Chen *et al.* reported that the direct conversion of solar energy into energy fuels and chemical energy is a promising green and sustainable approach to addressing the impending energy and environmental crises<sup>[16-23]</sup>. Qi *et al.* reported that these processes, known as photocatalysis, utilize suitable semiconductors and solar light to drive a variety of catalytic reactions, including the selective synthesis of organic compounds from liquid organic wastewater<sup>[24-30]</sup> and water splitting to produce H<sub>2</sub><sup>[31-42]</sup>.

The groundbreaking 1972 paper by Fujishima and Honda marked a significant milestone in the field of photocatalytic water splitting using TiO<sub>2</sub> electrodes under ultraviolet (UV) light<sup>[43]</sup>. Since then, numerous studies have reported significant progress in the fabrication of highly efficient semiconductor-based photocatalysts<sup>[44-51]</sup>. According to a literature review by Alam *et al.*, numerous photocatalysts have been developed that are active under both visible and UV light, including Ag<sub>3</sub>PO<sub>4</sub>/Mn-ZnO<sup>[52]</sup>, ZnO/MoO<sub>3</sub><sup>[53]</sup>, Al and Fe co-doped ZnO<sup>[54]</sup>, Ag<sub>2</sub>O/Fe-TiO<sub>2</sub><sup>[55]</sup>, Fe<sub>2</sub>O<sub>3</sub> doped TiO<sub>2</sub><sup>[56]</sup>, ZnO/CuO/MoO<sub>3</sub><sup>[57]</sup>, Bi<sub>2</sub>WO<sub>6</sub> modified by N-doped g-C<sub>3</sub>N<sub>4</sub><sup>[58]</sup>, Bi<sub>2</sub>WO<sub>6</sub> with Bi-metal and Bi<sub>2</sub>O<sub>3</sub><sup>[59]</sup>, BiVO<sub>4</sub>/TiS<sub>2</sub><sup>[60]</sup>, BiVO<sub>4</sub><sup>[61]</sup>, Ta<sub>2</sub>O<sub>5</sub><sup>[62,63]</sup>, TaON<sup>[64]</sup>, BiFeO<sub>3</sub><sup>[65]</sup>, Au/HCN and Au/BCN<sup>[66]</sup>, CdS<sup>[67]</sup>, and many others. Currently, there is significant interest in developing exceptional semiconductor photocatalysts to address environmental risks and energy scarcity. Sun *et al.* recently focused on designing visible-light-responsive photocatalysts that efficiently utilize the solar spectrum, which contains a significant portion of visible light (about 43%)<sup>[68-70]</sup>. However, conventional semiconductor photocatalysts, such as TiO<sub>2</sub>, possess a wide band gap energy that limits their effective utilization of solar energy, which is a major constraint for visible-light applications<sup>[71-73]</sup>. The band gap is a fundamental property of semiconductors that influences their electrical and optical properties. Bie *et al.* conducted an in-depth study on various aspects of photocatalytic full water splitting, both theoretically and practically, and concluded that although this technology presents significant challenges, it is likely to continue facing these challenges in the future<sup>[31]</sup>. In contrast, combining hydrogen (H<sub>2</sub>) production via photocatalysis with synergistic organic synthesis is a more feasible and attractive approach. This strategy is also a key focus of future research on dual-function photocatalysts<sup>[24,74]</sup>. As illustrated in Figure 1, this technology is gradually gaining public attention and holds the potential to enable organic synthesis from wastewater or liquid organic waste while concurrently producing hydrogen through the photocatalytic decomposition of water. Additionally, it helps mitigate environmental pollution and reduce the costs associated with the use of sacrificial agents. However, unlike typical studies in which hydrogen production and organic synthesis procedures are conducted independently, research on photocatalytic hydrogen production coupled with synergistic organic synthesis presents unique challenges and complexities. A dual-functional photocatalyst must simultaneously facilitate reactions that yield two outputs, a highly challenging task that is distinct from various organic synthesis operations where diverse catalyst materials exhibit varying physical and chemical properties<sup>[75,76]</sup>.



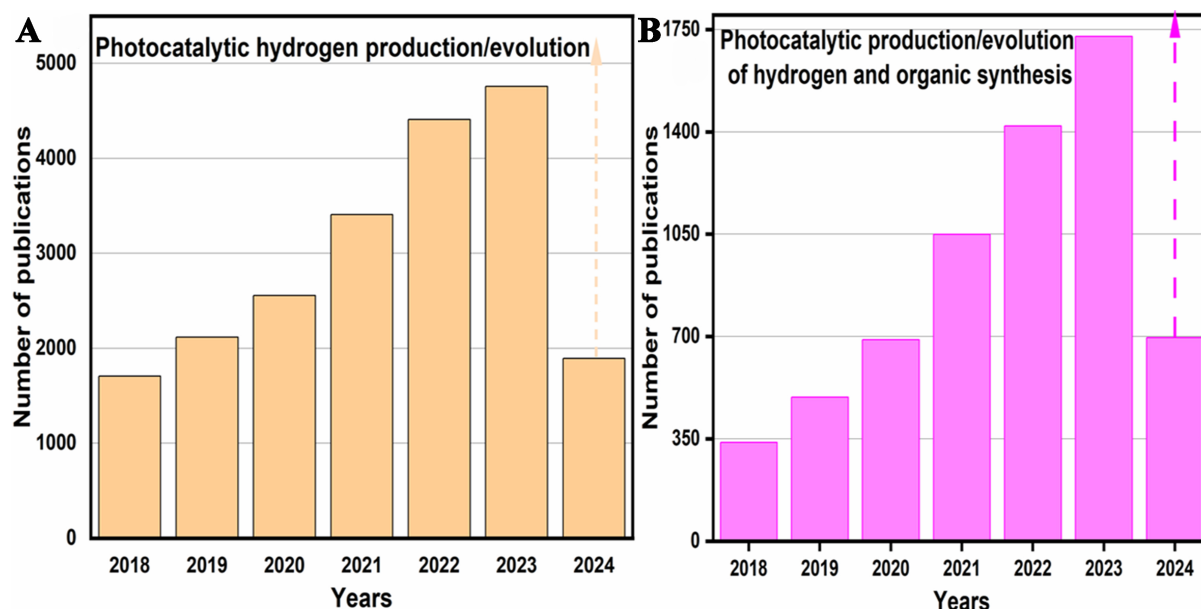


**Figure 1.** A number of publications related to (A) photocatalytic hydrogen production/evolution and (B) photocatalytic hydrogen production/evolution with synergistic organic synthesis from April 1, 2018, to May 19, 2024. Data were retrieved from ScienceDirect using relevant keywords.

Photocatalytic hydrogen generation coupled with synergistic organic synthesis from wastewater/liquid organic waste enables the control of reaction parameters and catalytic materials to meet specific requirements for organic synthesis or product preparation. Considering bi-functional synergy, this approach suggests a bi-directional selectivity between the photocatalyst and the waterborne contaminant. Enhanced hydrogen production coupled with simultaneous organic synthesis requires a suitable environment, the presence of a pollutant in water, and an effective catalyst. Essentially, the environmental medium, pollutants, and catalyst must be well-matched<sup>[24,77-79]</sup>. However, to the best of our knowledge, there is currently no concise summary of photocatalysis for H<sub>2</sub> production and synergistic organic synthesis from wastewater. Therefore, providing a timely and concise overview of the latest advancements in dual-functional photocatalytic systems is crucial.

In conclusion, this mini-review provides an overview of recent research on photocatalytic hydrogen production and organic synthesis from wastewater or liquid organic waste. This study highlights recent advancements in nanophotocatalyst material composition, microstructures, synthesized compounds, pollutant properties, reaction products, and co-existing materials in systems. In addition, the necessary techniques from both the catalyst and pollutant perspectives are discussed. Finally, this review summarizes the key challenges and prospects for future research directions in this promising field.

## FUNDAMENTAL PRINCIPLES OF PHOTOCATALYTIC MECHANISMS

### Overall water splitting

Titanium dioxide (TiO<sub>2</sub>), the first photocatalyst reported by Fujishima and Honda in 1972, has been extensively studied for its ability to induce light-driven water splitting<sup>[43,78,80]</sup>. Since then, TiO<sub>2</sub> and other semiconducting materials have been the focus of numerous photocatalysis studies<sup>[81,82]</sup>. Figure 2A illustrates the principles of overall water splitting (OWS) into H<sub>2</sub> and O<sub>2</sub> using a single semiconducting material in solution<sup>[83,84]</sup>. Firstly, according to the thermodynamics of this reaction, the conduction band (CB) minimum of the semiconductor must be more negatively potentialized than the H<sup>+</sup>/H<sub>2</sub> energy level [-0.41 V vs. normal

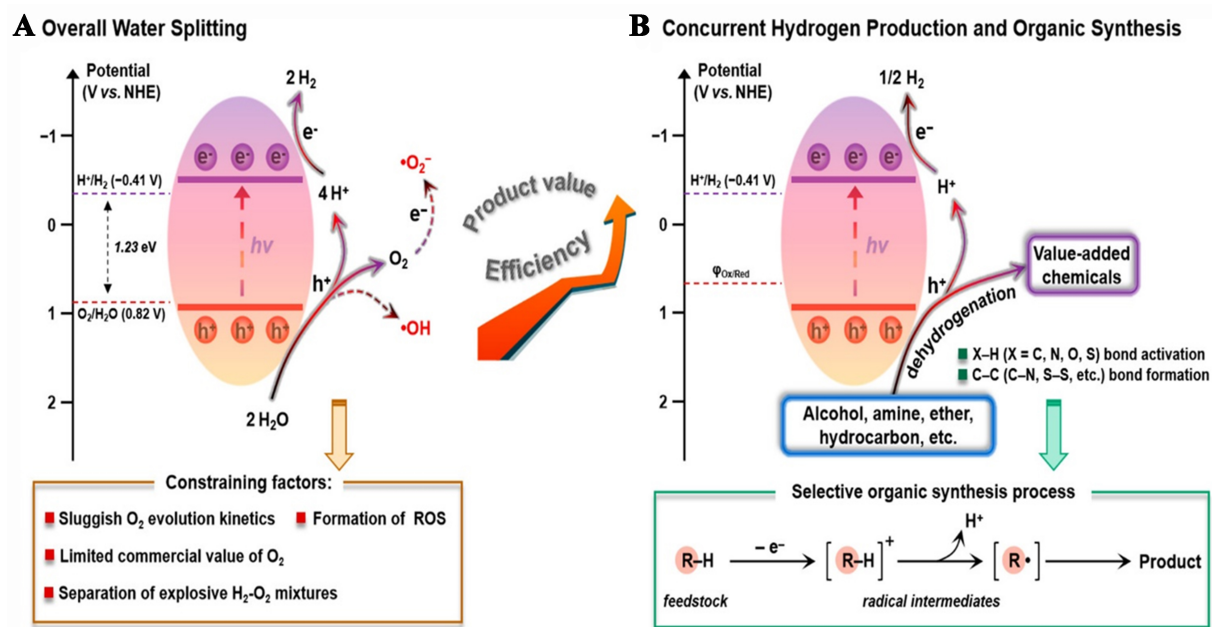


**Figure 2.** Diagram illustrating (A)  $H_2$  production via water splitting reaction and (B) the simultaneous coupling of  $H_2$  generation with selective organic synthesis over semiconductor-based photocatalysts<sup>[24]</sup>. Copyright 2021, American Chemical Society.

hydrogen electrode (NHE)], and the valence band (VB) maximum must be more positively potentialized than the  $O_2/H_2O$  energy level (0.82 V vs. NHE) for the two redox half-reactions to occur simultaneously<sup>[85]</sup>. Consequently, the semiconductor bandgap must be at least 1.23 eV for OWS. However, in practical applications, a bandgap larger than 1.7 eV is typically required because of the significant overpotential associated with the slowest kinetics of the water oxidation and proton reduction reactions. Secondly, the coupling of  $2e^-$  with  $2H^+$  is involved in the  $H_2$  evolution reaction (HER), which occurs more efficiently when semiconductor photocatalysts are coupled with HER cocatalysts<sup>[86]</sup>. The main challenge lies in the release of diatomic  $O_2$ , which requires the cleavage of four O-H bonds and subsequent production of O=O bonds. Typically, this process proceeds at reasonable rates only at high potentials<sup>[87]</sup>. Furthermore,  $O_2$  is a significant electron acceptor that opposes the HER half-reaction and produces reactive oxygen species (ROS), which can damage the system when water oxidation or  $O_2$  reduction occurs excessively<sup>[88]</sup>. Consequently, the conditions for initiating OWS are strict; failure to meet even one of the requirements prevents the reaction from occurring.

#### Photocatalytic hydrogen production with synergistic organic synthesis

Photocatalytic hydrogen production with synergistic organic synthesis from wastewater or separate photocatalytic organic synthesis requires several essential steps. These processes include (i) light absorption, (ii) formation and separation of electron-hole pairs, and (iii) surface reactions such as redox processes<sup>[78,89-91]</sup>. As illustrated in Figure 2B, the band gap represents the region between the VB and CB, where the density of state (DoS) is zero. The bandgap energy of semiconductors is smaller than that of insulators and is well-matched with the energy of photons in the solar spectrum. This enables photons to stimulate electron transitions within the semiconductor, generating electron-hole pairs that further drive photocatalytic reactions<sup>[92]</sup>. In addition, as illustrated in Figure 2B, the appropriate use of organic substrates, such as alcohols, hydrocarbons, ethers, and amines, as proton sources are essential for the synergistic reactions of hydrogen evolution and organic synthesis. Specifically, the X-H bonds (where X = C, N, O, and S) of organic reactants are activated and cleaved by holes with oxidizing ability. This process generates an

intermediate radical and a proton. The protons subsequently combine with photoexcited electrons in a reduction reaction to produce hydrogen. Intermediate radicals tend to recombine or reform C–C or C–X bonds, resulting in the formation of chemicals or other value-added oxidation products ( $O_x$ )<sup>[93–95]</sup>. **Figure 3** illustrates that visible light constitutes approximately 46% of sunlight, which is significantly greater than the 5% UV light. Visible light is also more readily absorbed and utilized than infrared light, which comprises approximately 49% of sunlight. Therefore, photocatalytic materials must improve their ability to absorb both visible and near-infrared light<sup>[96–98]</sup>. For effective photocatalytic processes, the photogenerated carriers must possess a sufficiently long lifetime to migrate to the catalyst surface, which is commonly referred to as the reaction active site. A key aspect of the photocatalytic implementation of this process is minimizing the recombination rate of the photogenerated electrons and holes. Following the migration of photogenerated carriers to the reaction sites, surface redox reactions occur. Here, photogenerated electrons reduce the number of active protons to produce hydrogen gas, while photogenerated holes or other strongly oxidative species gradually decompose synthetic materials into various intermediates or organic compounds, along with water. In these reactions, the photocatalytic mechanism, nature of the synthetic materials, and any co-existing substances all play critical roles in determining the overall efficiency and outcome of the process<sup>[31,78]</sup>.

#### *Concurrent organic synthesis and hydrogen production*

Any photocatalyst with an appropriate band structure can achieve the desired hydrogen evolution and organic oxidation. For dual-functionality, the photocatalyst must possess a sufficiently positive VB to drive the target organic oxidation and a CB that is more negative than the hydrogen production potential ( $-0.41$  V vs. NHE; pH = neutral). As illustrated in **Figure 4**, materials such as  $TiO_2$ , ZnO,  $Cu_2O$ , CdS, and  $g-C_3N_4$  possess sufficiently positive VB potential to oxidize most typical organic compounds, including alcohols, thiols, hydrocarbons, amines, and heterocycles<sup>[29,30,99]</sup>. The oxidation products of organic compounds are also determined by the VB of semiconductors. A semiconductor with an excessively positive VB, often indicating an excessively strong oxidation capacity, is not suitable for target organic synthesis. For example,  $TiO_2$  and ZnO, which possess wide band gaps, are commonly used to oxidize alcohols into aldehydes, ketones, or even mineralized compounds such as CO,  $CO_2$ , and  $H_2O$ <sup>[100,101]</sup>. In contrast, alcohol oxidation reactions often yield products involving carbon-carbon (C–C) linkages when visible light-active photocatalysts with narrow band gaps, such as CdS, are used<sup>[102,103]</sup>. Techniques such as doping, defect engineering, and crystal facet modifications enable the tuning of semiconductor band structures to optimize their photocatalytic performance<sup>[99,104]</sup>. This indicates that the band structures of photocatalysts can be tailored to promote specific organic oxidation reactions. However, a detailed discussion of these techniques is not explored further here because they have been comprehensively addressed in previous studies focused on hydrogen evolution and other single-function processes<sup>[92,105]</sup>. The energy levels of distinct semiconductor photocatalysts and the redox potential of different reactions in water-based solutions are shown in **Figure 4**<sup>[106]</sup>.

The primary objective of this review is to provide a comprehensive overview of recent advancements in the synergistic integration of high-value organic molecule synthesis and photocatalytic hydrogen production. To enhance this synergy, each subsection is organized based on specific photocatalysts, introducing several novel photocatalysts and innovative promotional strategies. The subsections address the characteristics of the photocatalysts, methods for catalyst modification, and factors influencing the activity and selectivity of these photocatalytic systems.

#### *Experimental photoreaction systems*

The experimental photoreaction system for hydrogen production and organic synthesis was conducted

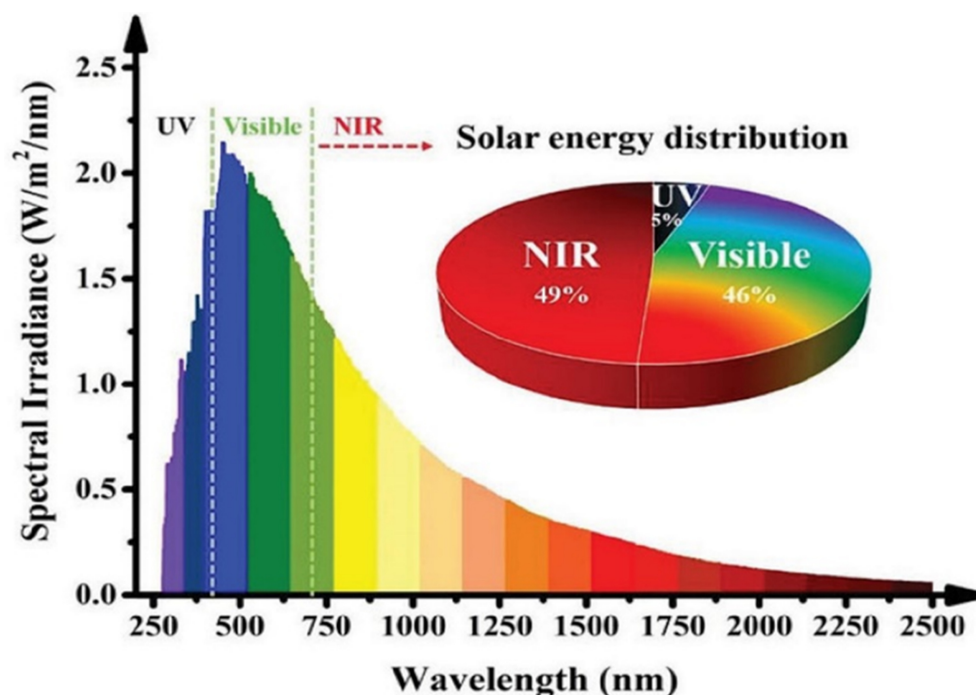


Figure 3. Standard solar energy distribution and solar radiation spectrum<sup>[98]</sup>. Copyright 2021, Wiley-VCH GmbH.

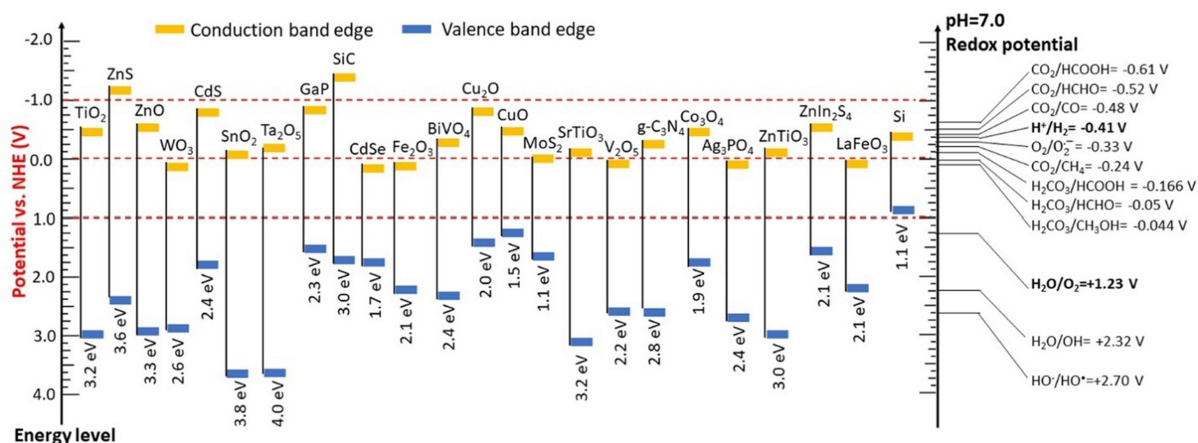


Figure 4. Energy levels of distinct semiconductor photocatalysts and the redox potential of different reactions in water-based solutions<sup>[106]</sup>. Copyright 2022, Elsevier B.V. All rights reserved.

under an argon atmosphere using a xenon lamp (PLS-SXE300) as the irradiation source at an intensity of 200 mW/cm. The reaction mixture, comprising 50 mL of aqueous solution, 5 mg of photocatalyst, and 0.5 mL of alcohol, was fully degassed and stirred for 1 h at 8 °C in the dark. Liquid products were analyzed using high-performance liquid chromatography (HPLC) equipped with a UV detector at 256 nm and a mobile phase consisting of 25% acetonitrile and 75% water. Gaseous products were quantified using gas chromatography. This experimental setup provides a suitable environment for investigating the efficacy of photocatalytic reactions in green chemistry.

### Difficulties and challenges in hydrogen production with synergistic organic synthesis

Although extensive research has been conducted on photocatalytic organic synthesis and hydrogen production from wastewater, synergistic catalysis remains relatively understudied. The primary challenge in achieving dual-function photocatalysis systems is that conventional photocatalytic hydrogen production typically occurs in an anaerobic environment. Under such conditions, oxygen captures the electrons generated by photosynthesis, which are essential for proton reduction, thereby influencing the subsequent hydrogen production reaction.

Photocatalytic organic synthesis from wastewater can be conducted in both aerobic and anaerobic environments. However, aerobic conditions may lead to unwanted side reactions, oxidation, or reduction of specific organic molecules when they interact with oxygen. To protect these sensitive molecules and enhance the selectivity of the desired transformations, anaerobic environments are often preferred. Anaerobic conditions can be achieved through oxygen-scavenging techniques or by purging reaction vessels with inert gases such as argon or nitrogen<sup>[107]</sup>. Conversely, many organic synthesis reactions can proceed in the presence of oxygen in an anaerobic environment. Many synthetic processes in laboratories and industries operate under aerobic conditions. In several transformations, oxygen serves as an oxidant, co-reactant, or oxygen atom source. For instance, molecular oxygen is typically required for oxidation reactions, epoxidation, hydroxylation, and oxidative coupling reactions. The synthesis of oxygen-containing functional groups, such as alcohols, ketones, and carboxylic acids, is often favored under aerobic conditions<sup>[108]</sup>.

In summary, organic synthesis can be performed in either anaerobic or aerobic environments, depending on the reaction type, substrate and intermediate reactivity, and desired products. To achieve efficient and selective outcomes, researchers and synthetic chemists carefully evaluate these factors when designing synthetic pathways and selecting appropriate reaction conditions. Integrating the two procedures requires not only an anaerobic environment, appropriate reaction conditions, and suitable reaction vessels but also ensures that the efficiency of organic synthesis and hydrogen production is maintained without mutual interference. However, the optimal conditions for such integrated systems require further investigation<sup>[109]</sup>.

Dual-function photocatalysis encounters challenges similar to those of traditional mono-functional photocatalysis, although under more demanding conditions. Materials with large bandgaps are more stable but exhibit limited visible-light absorption. Conversely, narrow-bandgap materials, although effective light absorbers, often suffer from low energy consumption and instability, thereby compromising the overall photocatalytic performance. This significantly reduces the efficiency of solar energy conversion<sup>[24,78,110]</sup>. As shown in Figure 5<sup>[111]</sup>, simultaneous oxygen-hydrogen production and organic synthesis can be achieved by carefully tuning various parameters, including catalyst type, dosage, and composition, as well as the microstructure, pollutant type and concentration, system interactions, pH, reaction temperature, and light intensity. The effects of the composites, additional catalyst components, and microstructures are particularly significant at the catalyst level. This section explores these aspects to reveal the underlying mechanisms that enable and enhance these processes.

### SYNTHESIS METHODS FOR NANO PHOTOCATALYSTS

The synthesis of nanophotocatalysts is crucial for modifying their properties and enhancing their catalytic performance. This section reviews both conventional and advanced synthesis methods, including sol-gel, solvothermal/hydrothermal, and precursor techniques, which are widely employed to control particle morphology, composition, and functionality. These approaches are fundamental for optimizing the photocatalytic properties of materials.



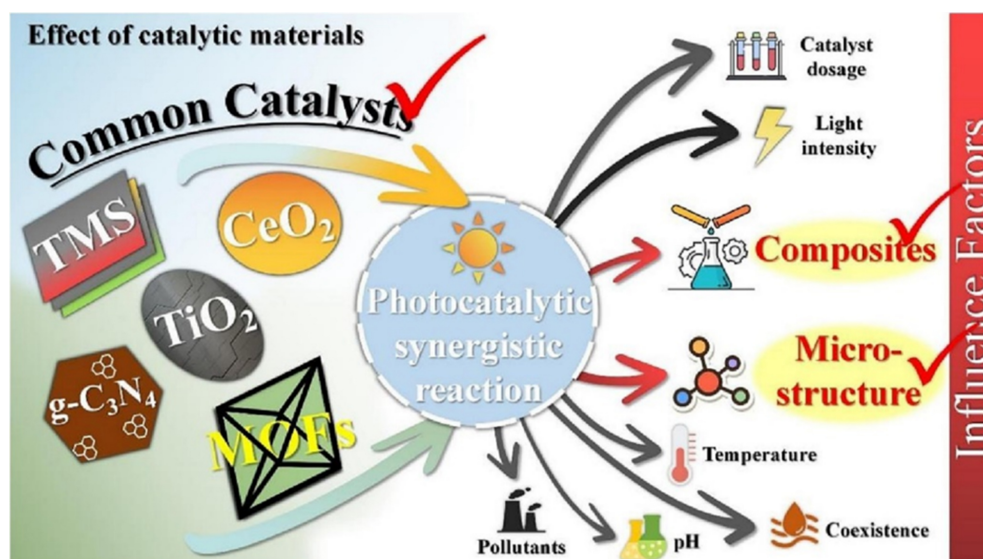


Figure 5. Effective aspects of synergistic photocatalytic reactions<sup>[111]</sup>. Copyright 2023, Elsevier B.V. All rights reserved.

Although physical synthesis methods are cost-effective, versatile, and allow for large-scale nanoparticle production, they often lack precise control over morphology and can introduce contaminants, which can adversely affect photocatalytic efficiency<sup>[112]</sup>. Chemical methods such as sol-gel and hydrothermal synthesis offer superior control over the size, shape, and surface properties of nano-photocatalysts, significantly enhancing their catalytic activity. These methods also enable synthesis in both aqueous and non-aqueous media, broadening their applications in biomedical and environmental fields<sup>[113,114]</sup>. However, challenges such as precursor toxicity and agglomeration can impact the material's properties and performance<sup>[115]</sup>. The following chemical and physical methods are used for particle synthesis, as illustrated.

### Sol-gel method

Sol-gel methods are synthetic techniques used to produce nanophotocatalysts. This chemical technique involves a combination of chemical and physical processes, including drying, calcination, dehydration, hydrolysis, and gelation. The term “sol-gel” refers to the transition of the solution into a “gel” during synthesis, characterized by an increase in viscosity, which is a distinctive feature of the method. Subsequent treatments facilitate the conversion of the gel into solid oxides<sup>[116]</sup>.

Metal alkoxides and alkoxy silanes are commonly used as precursors in this method. These colloids appear bulky when mixed with liquid, whereas the particles appear clear. The resulting gel exists in a continuous liquid phase. Compared to other techniques, sol-gel methods offer advantages such as cost-effectiveness, better product size, controlled morphology, low processing temperatures, high purity, and improved homogeneity. Both crystalline and noncrystalline materials can be synthesized using sol-gel techniques<sup>[117]</sup>. Figure 6 provides a visual representation of the proposed method<sup>[118]</sup>.

### Hydrothermal method

Among the various synthesis methods, the hydrothermal approach has been widely used for the production of nanophotocatalysts. The method is based on the solubility of many oxides in alkali-metal solutions. In this technique, water is used as a solvent due to its ability to dissolve minerals under high-pressure conditions, facilitating the formation of single crystals. Although effective, this synthesis method is time-consuming. An autoclave is used for crystal growth, where a nutrient is dissolved in water to facilitate the



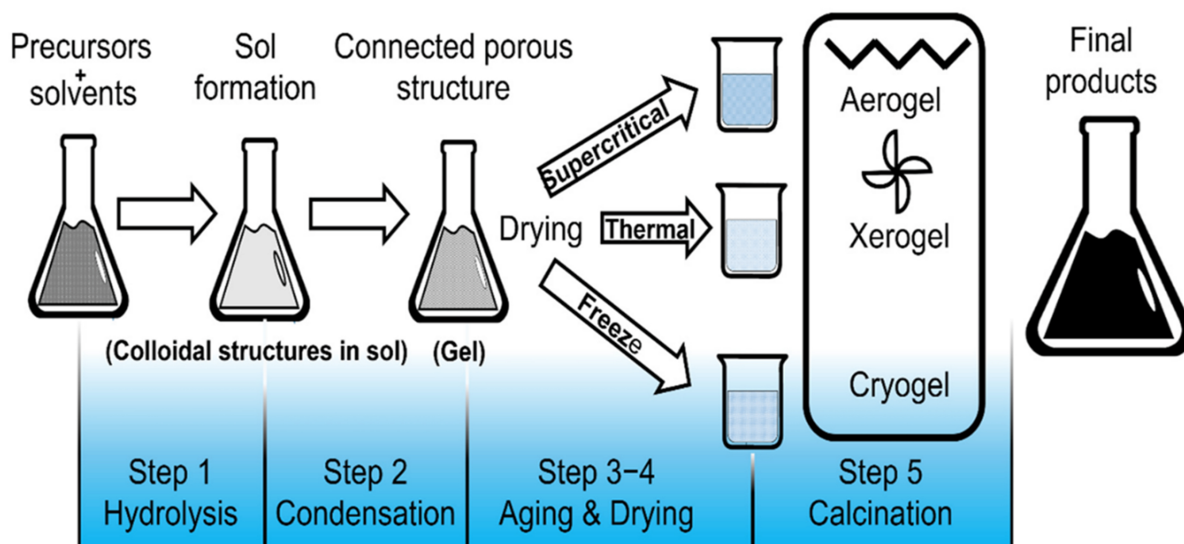


Figure 6. Schematic illustration of the sol-gel method<sup>[118]</sup>.

process. A schematic representation of the hydrothermal method used to fabricate metal oxide nanomaterials is shown in Figure 7<sup>[119]</sup>.

This method is also used for material recrystallization. A temperature gradient is maintained across the growth chamber, with the cooler end promoting crystal growth and the hotter end dissolving the nutrient supply. Hydrothermal methods also enable the monitoring of grain size and morphology. Their additional advantages include the ability to form crystalline phases and control the composition to grow high-quality crystals. However, autoclaves are expensive, and real-time crystal growth monitoring is not feasible<sup>[120]</sup>.

### Solvothermal method

Solvothermal synthesis is a widely used method for producing nanophotocatalysts and other chemical compounds. This process is similar to hydrothermal synthesis, but the primary difference lies in the type of precursor used. While the hydrothermal method uses an aqueous solution (water), it uses a non-aqueous solution, such as alcohol or amine, as the precursor. The reaction proceeds within this solvent at temperatures exceeding its boiling point, leading to the formation of single crystals under high temperatures in a non-aqueous solution within the autoclave. This technique enables the formation of particles with precise and controlled shapes, improved morphologies, well-defined crystallinities, and phase distributions. The major advantage of solvothermal synthesis is its ability to combine the benefits of hydrothermal and sol-gel methods<sup>[121,122]</sup>. The solvothermal method is analogous to the hydrothermal approach; thus, the same schematic representation shown in Figure 7 can be applied.

### Ceramic method

The ceramic method is widely used to synthesize mixed metal oxides, nano-photocatalysts, and various metals, along with phosphides, metal sulfates, and nitrides of different metals. It involves high-temperature processing, often achieved through resistance heating, which can influence the size, shape, and crystallographic properties of the resulting product. Powders of the desired material's oxides or other compounds are ground at these elevated temperatures, typically after pelletization. A diagrammatic representation of the ceramic synthesis process is shown in Figure 8<sup>[123]</sup>.

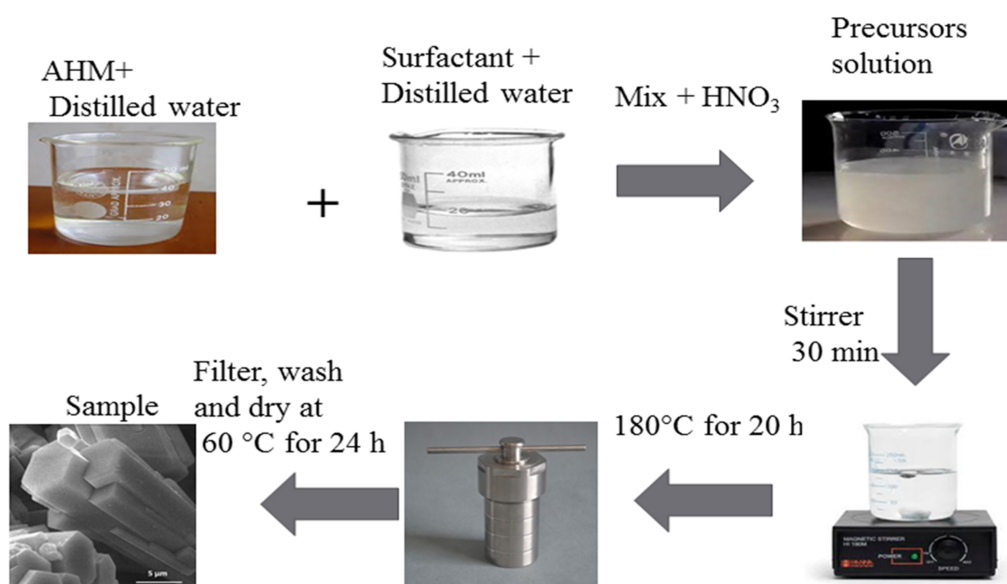


Figure 7. Hydrothermal methods for the fabrication of metal oxide nanomaterial<sup>[119]</sup>. Copyright 2021 Published by Elsevier B.V.

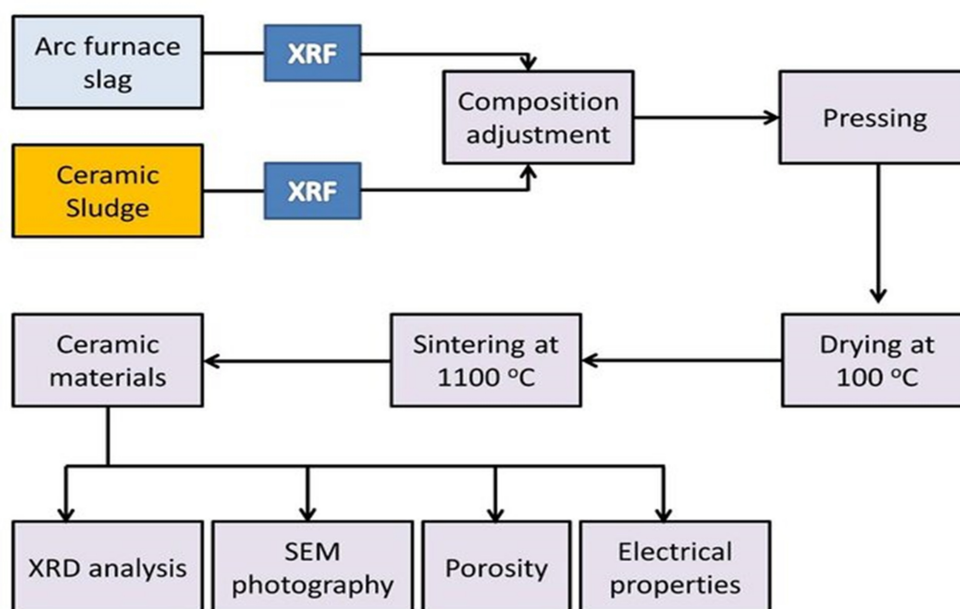


Figure 8. Flowchart of the ceramic synthesis process<sup>[123]</sup>.

However, this method has several disadvantages. It requires extremely high temperatures and lacks a monitoring procedure to determine when the reaction is complete, often relying on trial and error. Achieving a homogenous product composition is challenging, and after the reaction is complete, unreacted materials often remain as impurities and byproducts that cannot be separated from the desired product, compromising its purity and phase identification<sup>[124,125]</sup>.

### Co-precipitation method

The co-precipitation method is a widely adopted synthesis technique because of its simplicity, cost-effectiveness, and versatility. This time-consuming method involves the formation of “mixed precipitates”, consisting of two or more insoluble compounds that can be easily removed from the solution. Different classes of nanophotocatalysts have been synthesized through co-precipitation methods, including<sup>[126]</sup>:

- Mixed metal oxide nanoparticles such as ZnO, NiO, and CdO.
- Doped metal oxides.
- Ternary ferrites with the structure  $M\text{-Fe}_2\text{O}_4$ , where M represents a divalent metal ion.
- Mixed ferrites with two metals, having the composition  $A_{1-x}B_x\text{Fe}_2\text{O}_4$ .

Divalent metal cations, such as nitrates, sulfates, and chlorides, are mostly inorganic salts that are readily soluble in water. Precipitating agents, usually acidic or basic compounds such as NaOH,  $\text{NH}_3$ , citric acid, and polyethylene glycol (PEG), are used to extract the byproduct from the solution and form the desired nanophotocatalysts precipitates. The precipitates are subsequently calcined in a muffle furnace to form spinel nanocomposites. During synthesis, the pH is maintained between 9 and 11 to facilitate the formation of high-quality crystals. Figure 9 shows a schematic representation of this process<sup>[127]</sup>.

The crystal growth of these particles is influenced by factors such as temperature, pH of the material and synthesis solution, composition, and salt concentration. After precipitation, the solid was allowed to settle and washed repeatedly with ethanol and distilled water. This washing process must be performed carefully to prevent particle agglomeration, which can adversely affect the morphology and structural properties of the nanophotocatalysts<sup>[128]</sup>. This can be minimized by maintaining a neat and clean working environment. After washing, the solid material is dried at the melting temperature for several hours and then finely ground to form a powder. The powder is then calcined at temperatures ranging from 550 to 800 °C, depending on the material. If necessary, a sintering process can be conducted, depending on the nature of the prepared material. The calcination temperature and duration are crucial factors affecting the particle size and surface morphology of the final product.

The co-precipitation method offers several advantages, including<sup>[129]</sup>:

- Lower temperature requirements than those of other techniques
- Cost-effectiveness
- Formation of fine, uniform particles with reduced agglomeration
- Homogenous and single-phase crystal formation

However, the chemical co-precipitation method is limited when dealing with materials exhibiting dissimilar solubility in water, including:

- Commonly occurring supersaturated solutions
- Different precipitation rates of reactants

Many researchers have adopted the co-precipitation method to synthesize nanoparticles of various material classes, making it one of the most common techniques for preparing nanophotocatalysts.

### Biosynthesis method

A biosynthetic method is a biological approach used to synthesize materials from various organisms, including algae, fungi, bacteria, and plants, for applications in medicine.

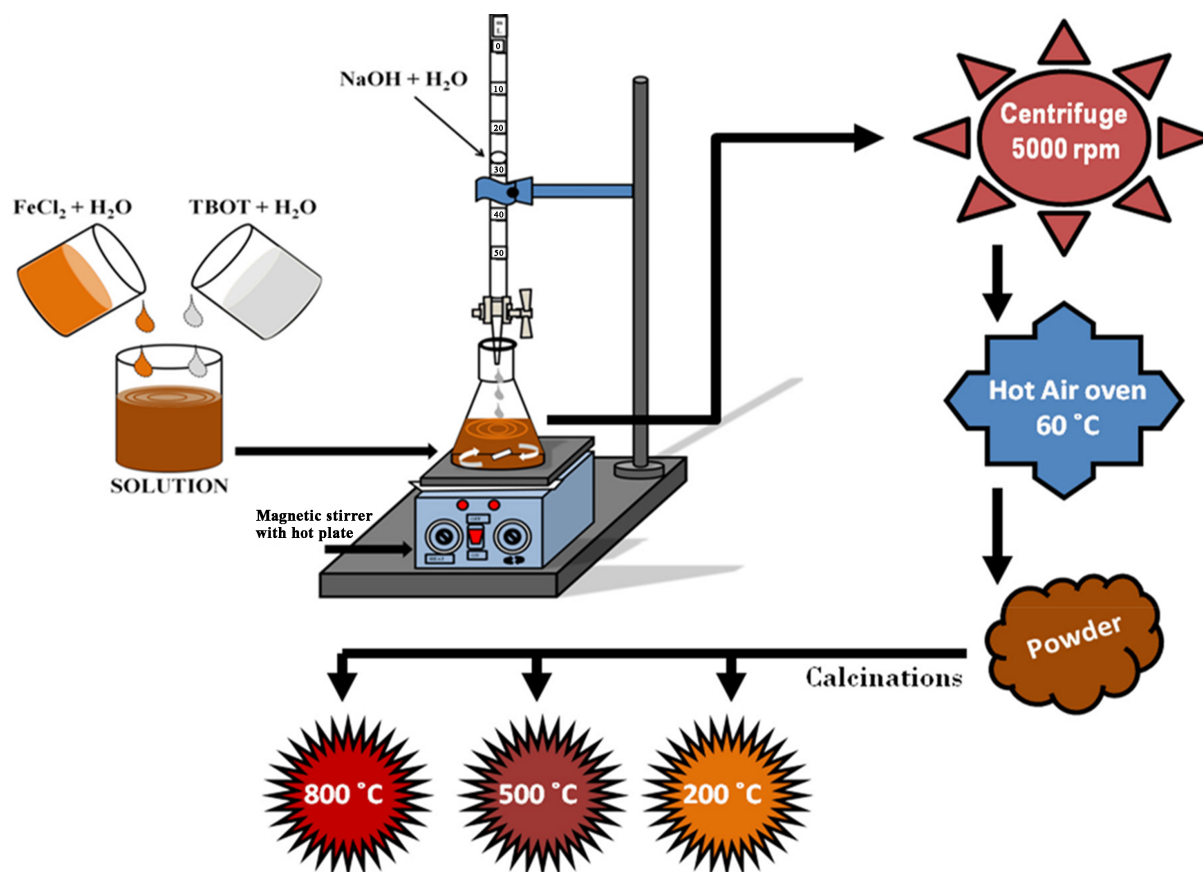


Figure 9. Schematic diagram of the co-precipitation technique<sup>[127]</sup>.

Recent advancements have led to the development of green synthesis methods for producing nanoparticles with the desired particle size and morphology. These methods employ stabilizing, reducing, and capping agents derived from biological sources such as plants, bacteria, fungi, and algae. By using these natural agents, it is possible to synthesize materials without relying on expensive, toxic, or harsh chemical precursors, making this approach environmentally friendly and sustainable. This approach is a simple and cost-effective synthesis route. Figure 10 shows a schematic representation of the biosynthesis of nanoparticles<sup>[130]</sup>. Currently, various types of particles, including sulfides, metals, metallic oxides, and ferrite, are synthesized using biosynthesis method. The samples prepared through biosynthesis have diverse applications, including DNA analysis, magnetic resonance imaging (MRI), biosensors, cancer treatment, gene therapy, material separation science, and drug delivery<sup>[131]</sup>.

### Spray pyrolysis method

In spray pyrolysis methods, micro-sized liquid droplets of a precursor material mixture are converted into solid particles through heat treatment. The process typically involves the following steps, as illustrated in Figure 11<sup>[132]</sup>:

- Generation of micro-sized droplets of precursor materials
- Solvent evaporation
- Solute condensation
- Reaction and decomposition of solutes
- Sintering of solid particles

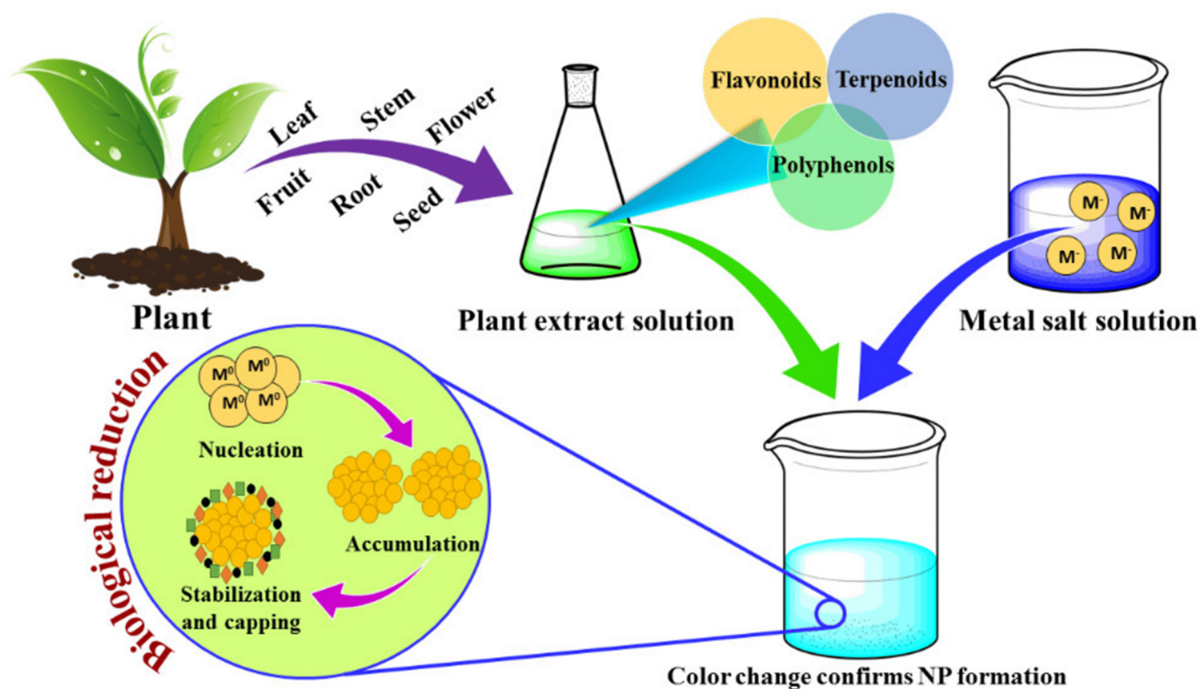


Figure 10. Graphic illustration of the plant-mediated biosynthesis of nanoparticles<sup>[130]</sup>.

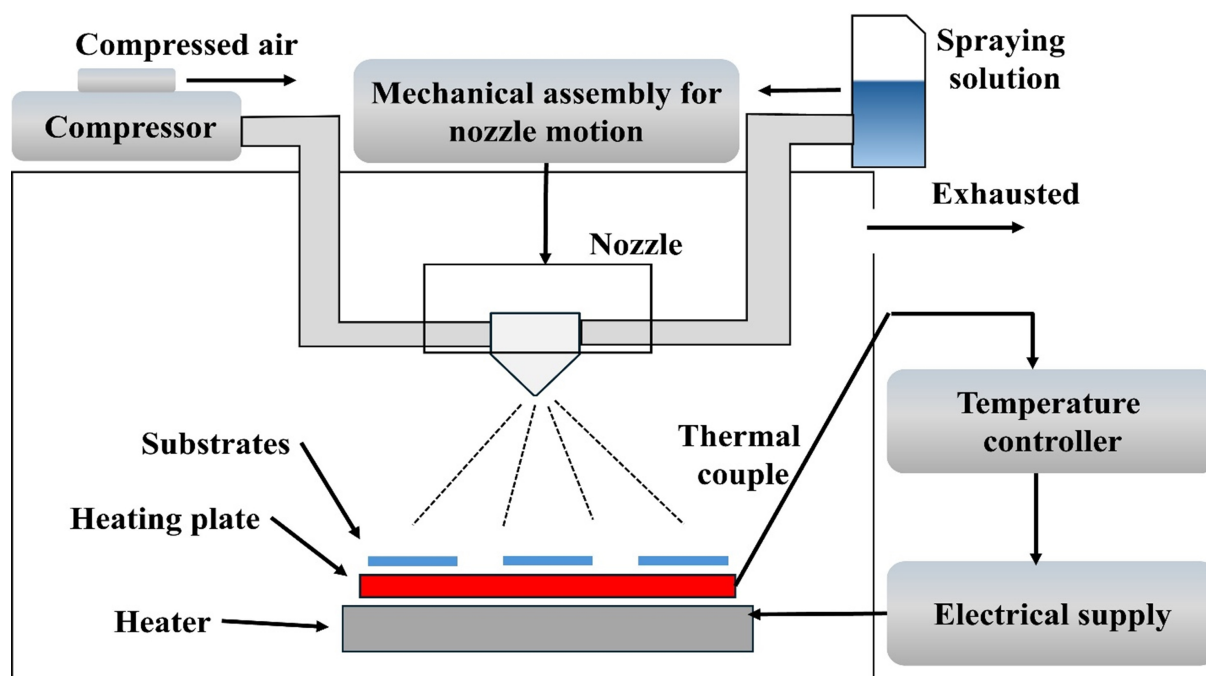


Figure 11. Representation of spray pyrolysis procedure and its apparatus<sup>[132]</sup>.

### Precursor method

In the precursor method, mixtures of metals and easily decomposable metal compounds are prepared. Upon heating, these metals form the desired oxides. The method allows the production of high-purity oxide materials with fine particles and a homogeneous composition and facilitates the preparation of



nanophotocatalysts from water-soluble salt solutions of the corresponding materials. It is employed to produce single-phase nanophotocatalyst materials with large surface areas, high purity, low porosity, and molecular-level homogeneity, as shown in [Figure 12](#)<sup>[133]</sup>.

### Solid-state reaction method

The solid-state reaction (SSR) technique is widely used to synthesize polycrystalline bulk materials, particularly manganites and ferrites. This method uses a range of starting materials, including sulfates, nitrates, oxides, and carbonates. The solid precursors are heated at elevated temperatures to facilitate the desired reaction at an appropriate rate, as solids typically do not react at ambient conditions. The high-temperature environment minimizes concerns of agglomeration or structural alterations during synthesis<sup>[134]</sup>.

The SSR method produces a stable product through chemical reactions between solid precursors in the absence of a solvent at high temperatures. A primary advantage of this route is that the obtained product is in solid form and exhibits uncontaminated structural properties that are influenced by the sintering temperature. Additionally, this method is environmentally friendly and nontoxic, as it does not generate unwanted waste or byproducts<sup>[135]</sup>.

A significant limitation of the SSR method is its inability to produce large single crystals. Additionally, it is energy-intensive and time-consuming, and it has low efficiency. The requirement for high temperatures and specialized furnaces further adds to the drawback of this method, as illustrated in [Figure 13](#)<sup>[135,136]</sup>.

## NANO PHOTOCATALYSTS FOR HYDROGEN PRODUCTION AND ORGANIC SYNTHESIS

Hydrogen is emerging as a promising clean and versatile energy source, attracting significant attention for its potential to replace fossil fuels in diverse applications such as fuel cells, energy storage, and transportation systems. Various types of nano-photocatalysts, including metal oxides, metal sulfides, carbon-based materials, and hybrid structures, have been effectively employed in hydrogen production and organic synthesis from wastewater and alcohol. The proposed approach offers a promising solution for treating wastewater while simultaneously generating sustainable energy. The use of nanostructured photocatalysts enhances the efficiency and selectivity of water-splitting processes. Recent advancements in nanophotocatalyst research and development have led to significant performance improvements, including reduced charge recombination losses, effective charge separation, and increased light absorption<sup>[137,138]</sup>. To enhance the catalytic activity of photocatalysts used in hydrogen evolution processes, various strategies have been employed, such as surface modification, heterostructuring, and doping<sup>[139]</sup>. These approaches aim to modify the electronic band structure and surface properties of catalysts. In addition to hydrogen production, nanophotocatalysts have attracted significant attention for their applications in organic synthesis. They facilitate the production of fine chemicals, pharmaceuticals, and biofuels from renewable energy sources. Photocatalytic organic transformations, such as oxidative coupling reactions, C-H functionalization, and C-C bond formation, enable the synthesis of complex organic molecules in an environmentally friendly and sustainable manner<sup>[102,140]</sup>. Nanostructured photocatalysts exhibit remarkable catalytic performance with excellent selectivity and moderate reaction conditions in various organic synthesis reactions. The precise control over reaction pathways and product distribution enabled by the regulated photocatalytic activation of organic materials facilitates the formation of valuable molecules with minimal environmental impact.

However, a comprehensive review of the literature on this topic is lacking. This overview summarizes the current state of the art based on a few recent publications. In recent years, there has been a significant surge



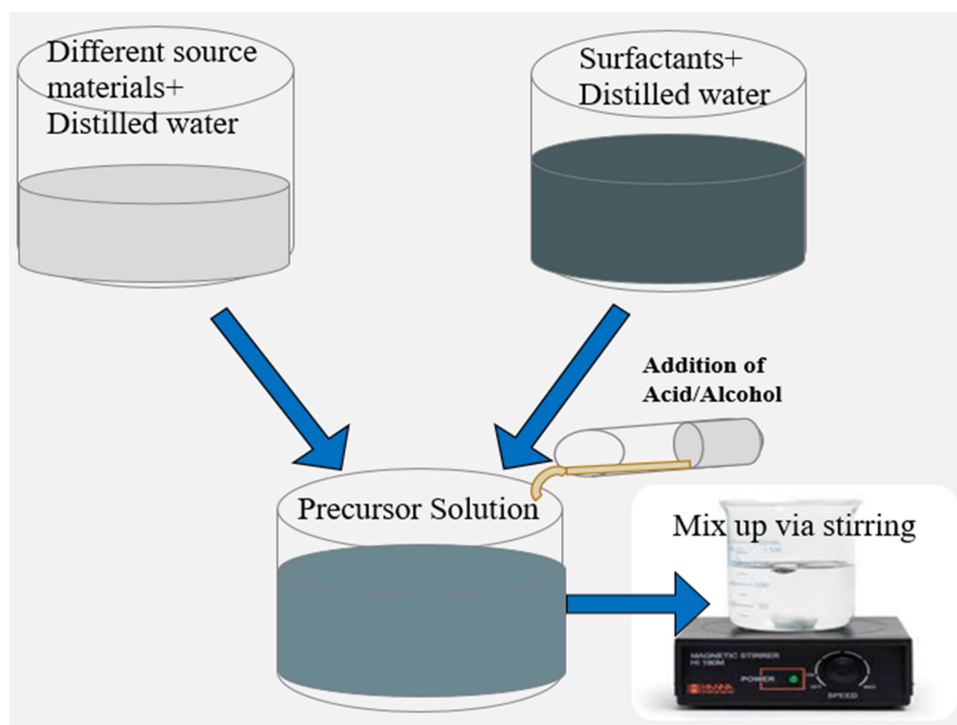


Figure 12. Fabrication procedure of a precursor solution.

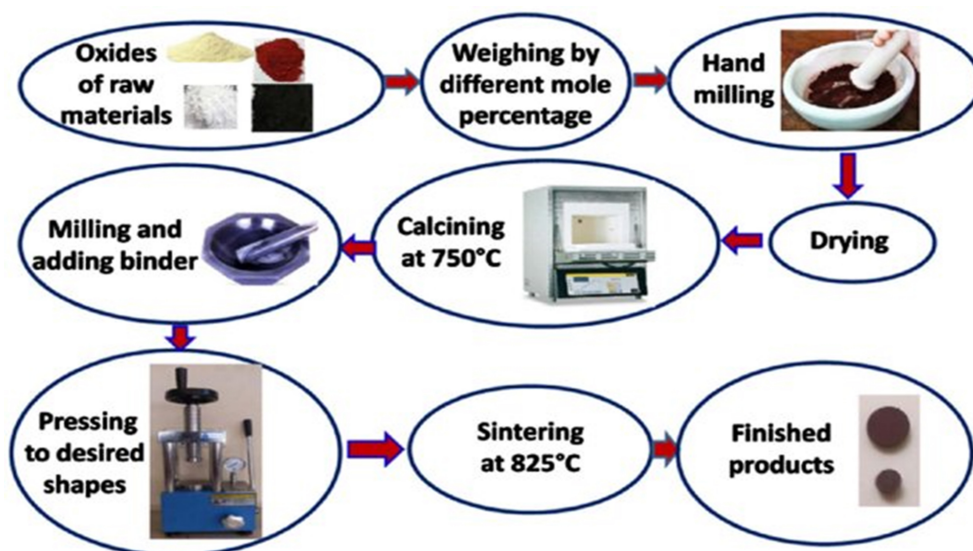


Figure 13. Graphic illustration presenting the diverse steps of the SSR method<sup>[136]</sup>. SSR: Solid-state reaction.

in interest in photocatalytic reactions for hydrogen production and organic synthesis. This is largely due to the unsustainable nature of traditional industrial methods for the synthesis of hydrogen and organic compounds, which have significant resource and environmental implications, as detailed in the literature and Table 1. Shang *et al.* demonstrated the potential of a 1D/2D CdS/BiVO<sub>4</sub> binary nanocomposite synthesized through electrostatic self-assembly for organic synthesis and hydrogen production. This composite effectively catalyzed C-C coupling with benzaldehyde as the substrate<sup>[141]</sup>. Similarly, Luo *et al.*

**Table 1. Summary of some reported research papers on photocatalytic H<sub>2</sub> production and organic synthesis**

Photocatalyst	Synthesis method	Morphology	Light source	Hydrogen production	Synthesized organic products	Ref.
MgO	Colloidal chemical	Porous type	Solar	320 $\mu\text{mol}\cdot\text{g}^{-1}\cdot\text{h}^{-1}$	Formaldehyde	[144]
Pt/TiO <sub>2</sub>	Sol-gel	Nano-film	UV-Vis	4.675 $\text{mmol}\cdot\text{h}^{-1}$	Formic acid	[145]
N-doped TiO <sub>2</sub> and Au-doped TiO <sub>2</sub>	Deposition precipitation	Nanoparticles	Visible	200 $\text{nmol}\cdot\text{g}^{-1}\cdot\text{h}^{-1}$	Methyl formate	[146]
2D SnS/g-C <sub>3</sub> N <sub>4</sub>	Hydrothermal	Nanosheets	Visible	1.27 $\text{mmol}\cdot\text{g}^{-1}\cdot\text{h}^{-1}$	Liquid chemicals	[147]
defective TiO <sub>2</sub>	Facile NaBH <sub>4</sub> reduction	Bulk crystal structure	UV and Visible	0.08 $\text{mmol}\cdot\text{h}^{-1}$	Liquid acetaldehyde	[149]
Ni-MMT/TiO <sub>2</sub>	Sol-gel	MMT layers on the spherical shape of TiO <sub>2</sub>	UV	3,470 $\mu\text{mol}\cdot\text{g}^{-1}\cdot\text{h}^{-1}$	Hydrocarbons	[150]
Au@TiO <sub>2</sub> (Ti <sup>3+</sup> )	Sol-gel	Nanoparticles and nanorods	Visible	~7,093 $\mu\text{mol}\cdot\text{g}^{-1}\cdot\text{h}^{-1}$	CH <sub>4</sub>	[151]
CdS/MOF	Hydrothermal	Block shaped	Visible	2,334 $\mu\text{mol}\cdot\text{g}^{-1}\cdot\text{h}^{-1}$	Benzaldehyde	[152]
Co/CdS	Photo-deposition	Nanorods	Visible	442 $\mu\text{mol}\cdot\text{g}^{-1}\cdot\text{h}^{-1}$	Benzaldehyde	[153]
AgNPs/CdS	Microwave-assisted	Rod-like linear structure	Visible	1,720.9 $\mu\text{mol}\cdot\text{g}^{-1}\cdot\text{h}^{-1}$	Acetaldehyde	[155]
Pd/HNb <sub>3</sub> O <sub>8</sub> -H <sub>2</sub>	Impregnation and thermal treatment	porous structure	Visible	3.17 $\text{mmol}\cdot\text{g}^{-1}\cdot\text{h}^{-1}$	Benzaldehyde	[104]
MOF-derived Co <sub>9</sub> S <sub>8</sub> /CdS	Hydrothermal	Pore type structure	Visible	61,924 $\mu\text{mol}\cdot\text{g}^{-1}$ in 6 h	Benzaldehyde	[157]
P and S-doped g-C <sub>3</sub> N <sub>4</sub>	Co-precipitation	Mesoporous spheres	Visible	3.76 $\mu\text{mol}\cdot\text{g}^{-1}\cdot\text{h}^{-1}$	Benzaldehyde	[158]
Pd <sub>SA+C</sub> /TiO <sub>2</sub> -V <sub>O</sub>	Pyrolysis	Rectangular blocks and clusters	UV-visible	5,800 $\mu\text{mol}\cdot\text{g}^{-1}\cdot\text{h}^{-1}$	N-benzylidenebenzylamine	[99]
MoS <sub>2</sub> /ZnIn <sub>2</sub> S <sub>4</sub>	Facile photochemical reduction	NFs	Visible	3.88 $\text{mmol}\cdot\text{g}^{-1}\cdot\text{h}^{-1}$	Benzaldehyde	[95]

UV: Ultraviolet; MMT: montmorillonite; MOF: metal-organic framework; AgNPs: silver nanoparticles; NFs: nanoflowers.

investigated a NiS/CdS nanorod composite for simultaneous H<sub>2</sub> production and benzaldehyde oxidation. The incorporation of NiS into CdS nanorods significantly enhanced electron-hole pair separation and overall stability, leading to improved photocatalytic performance<sup>[142]</sup>.

Pang *et al.* successfully synthesized single-layer MoS<sub>2</sub>, WS<sub>2</sub>, and ReS<sub>2</sub> nanosheets using a one-pot colloidal wet-chemical method. Different molecular surfactants were used to facilitate the growth of single-layer 2D morphologies. These nanosheets were subsequently utilized for H<sub>2</sub> fuel production through the decomposition of methanol into formaldehyde, derived from hydrogen-stored liquid waste containing methanol. MoS<sub>2</sub> exhibited the optimum photocatalytic efficiency, achieving approximately 617  $\mu\text{mol}\cdot\text{g}^{-1}\cdot\text{h}^{-1}$  under normal pressure and room temperature conditions. This approach offers a promising pathway for generating solar H<sub>2</sub> fuel by storing methanol, which can be easily produced through chemical re-bonding facilitated by 2D single-layer photocatalysts<sup>[143]</sup>.

Liu *et al.* developed a novel facile colloidal chemical method to synthesize MgO for H<sub>2</sub> production from liquid methanol at room temperature. The formation of CO<sub>x</sub>-free H<sub>2</sub> is also attributed to the photodecomposition of methanol into formaldehyde, facilitated by the surface electronic states of distinct monodispersed, porous MgO nanocrystals. The photocatalytic H<sub>2</sub> production performance of the MgO photocatalyst from methanol improved over time,

reaching  $320 \mu\text{mol}\cdot\text{g}^{-1}\cdot\text{h}^{-1}$  after 2 days. The energy band gap and charge carrier recombination decreased as the size of the MgO nanoparticles increased to  $170 \text{ nm}$ <sup>[144]</sup>.

Cui *et al.* fabricated a Pt/TiO<sub>2</sub> nano-film using the sol-gel method. In a continuous-flow reactor, the Pt/TiO<sub>2</sub> nano-film demonstrated photocatalytic decomposition of methanol aqueous solution into H<sub>2</sub> and formic acid. The study investigated the effects of several variables, including the methanol concentration, reaction duration, and space velocity, on the photocatalytic process. Notably, the photocatalytic activity of the Pt/TiO<sub>2</sub> nano-film exceeds that of pristine TiO<sub>2</sub><sup>[145]</sup>.

Gazsi *et al.* synthesized N- and Au-doped TiO<sub>2</sub> using the deposition-precipitation method. In all cases, the addition of H<sub>2</sub>O or O<sub>2</sub> to the alcohol reduced CO production; in the case of methanol, CO was entirely removed. The photocatalytic decomposition of methanol and ethanol into H<sub>2</sub> and methyl formate was significantly enhanced by Au-doped TiO<sub>2</sub> compared with N-doped TiO<sub>2</sub> under visible light<sup>[146]</sup>.

Uddin *et al.* synthesized 2D SnS/g-C<sub>3</sub>N<sub>4</sub> heterojunction photocatalysts using a hydrothermal method. The photocatalysts enhanced H<sub>2</sub> production and organic or liquid chemical synthesis from liquid organic waste, such as methanol, ethanol, and isopropanol, without the emission of CO<sub>x</sub>. The process achieved approximately 95% recoverability, and the hydrogen generation efficiency reached  $1.27 \text{ mmol}\cdot\text{g}^{-1}\cdot\text{h}^{-1}$ . Experimental and product analyses revealed that process reduction occurs through a series of redox processes, including disproportionation and combination. Each alcohol demonstrated a higher hydrogen production efficiency than previous reports, along with excellent reversibility (> 95%) over extended periods of operation (up to 360 h). In this study, the use of 2D SnS/g-C<sub>3</sub>N<sub>4</sub> heterostructures for phototransforming light alcohols exemplifies a selective reaction, as illustrated in Figure 14<sup>[147]</sup>.

Xie *et al.* prepared MoS<sub>2</sub> and CdS for the conversion of methanol into hydrogen and ethylene glycol (EG) through controlled C-C coupling, a highly desirable and promising goal. This work introduced a novel visible-light-driven catalytic C-H activation approach for EG synthesis that preserves the hydroxyl group within the same molecule while offering an alternative, non-petroleum-based method<sup>[84]</sup>.

Tan *et al.* developed bifunctionally modified carbon nitride incorporating interior cyano and surface carboxyl groups through a two-step process. This modification resulted in a photocatalyst with 205 times more active sites and an enhanced photoexcited charge carrier separation efficiency compared with pristine carbon nitride. The modified photocatalyst exhibited superior hydrogen and formaldehyde production performance in methanol-containing wastewater under visible light illumination<sup>[148]</sup>.

Zhang *et al.* developed a simple NaBH<sub>4</sub> reduction method to fabricate defective TiO<sub>2</sub> photocatalysts for the simultaneous production of H<sub>2</sub> gas and organic compounds such as acetaldehyde from methanol, ethanol, and isopropanol-containing wastewater. The modified TiO<sub>2</sub> exhibited enhanced light absorption and charge separation, leading to improved photocatalytic activity. This resulted in a hydrogen production rate of  $0.08 \text{ mmol/h}$  and high-purity (99%) liquid acetaldehyde, surpassing the performance of bare TiO<sub>2</sub>, as illustrated in Figure 15. Figure 16A and B provides a schematic representation of the photoreaction setup under UV and UV-visible light, respectively<sup>[149,150]</sup>.

Muhammad Tahir synthesized Ni and montmorillonite (MMT)-loaded TiO<sub>2</sub> (Ni-MMT/TiO<sub>2</sub>) nanocomposites using the sol-gel method. These nanocomposites exhibited significant photocatalytic activity for H<sub>2</sub> production and the generation of C<sub>1</sub>-C<sub>3</sub> or CH<sub>4</sub>/C<sub>2</sub>H<sub>6</sub>/C<sub>3</sub>H<sub>8</sub> hydrocarbons from ethanol-water mixture under UV light irradiation. The 3 wt% Ni-10 wt% MMT/TiO<sub>2</sub> nanocomposite exhibited the highest

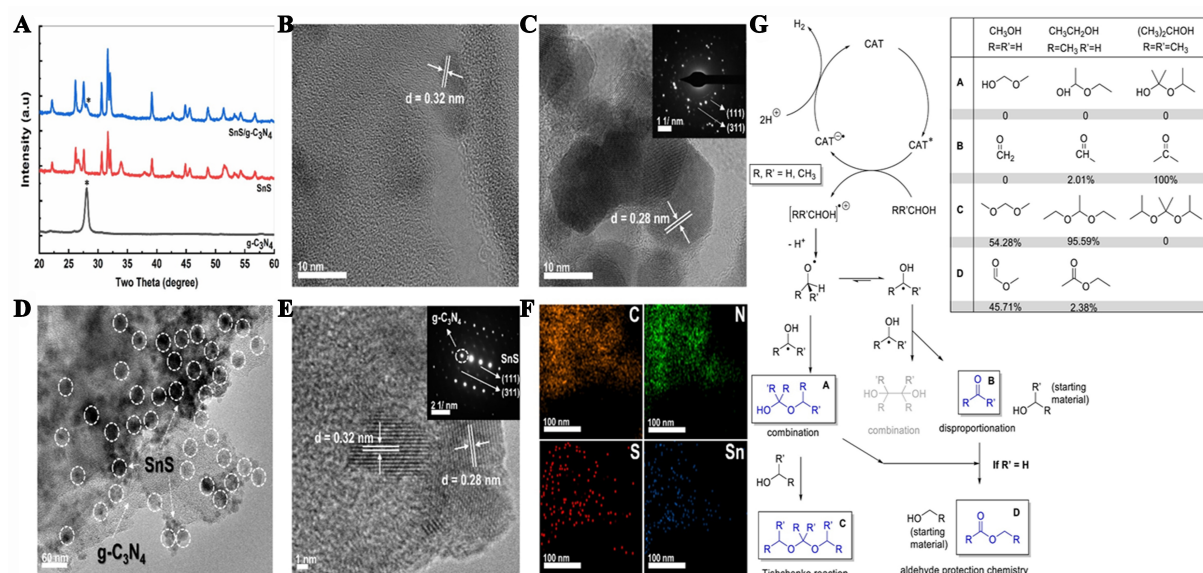


**Figure 14.** (A) Powder XRD and (B) HRTEM images of both g-C<sub>3</sub>N<sub>4</sub> and SnS; (C) Selected area electron diffraction results of SnS and SnS/g-C<sub>3</sub>N<sub>4</sub>; (D) EDS elemental maps of SnS/g-C<sub>3</sub>N<sub>4</sub> heterojunction; (E) HRTEM images of SnS/g-C<sub>3</sub>N<sub>4</sub>; (F) STEM with an EDS elemental map showing the co-existence of Sn, N, C, and S in the SnS/g-C<sub>3</sub>N<sub>4</sub> heterostructure; (G) Photo-oxidation of isopropanol, ethanol, and methanol along with experimental output ratios<sup>[147]</sup>. Copyright 2021, Elsevier B.V. All rights reserved. XRD: X-ray diffraction; HRTEM: high-resolution transmission electron microscopy; EDS: energy dispersive spectroscopy; STEM: scanning transmission electron microscopy.

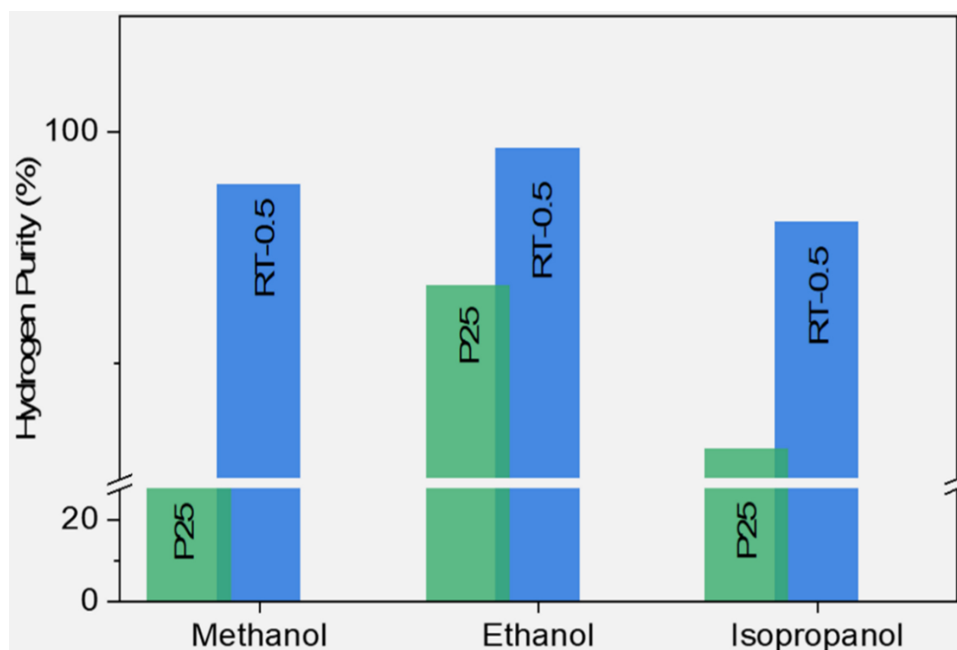


**Figure 15.** Hydrogen purity achieved using pristine and defective TiO<sub>2</sub> catalysts with various reactants<sup>[149]</sup>. Copyright 2023, Author(s). Published by Elsevier B.V.

H<sub>2</sub> production rate of 3,470 μmol·g<sup>-1</sup>·h<sup>-1</sup> with a selectivity of 99%. This performance is 2.62 times greater than that of Ni-doped TiO<sub>2</sub>, 6.48 times higher than MMT/TiO<sub>2</sub>, and 6.45 orders of magnitude higher than that of pure TiO<sub>2</sub>. To assess the lifespan and reusability of the composite catalysts, stability tests were conducted

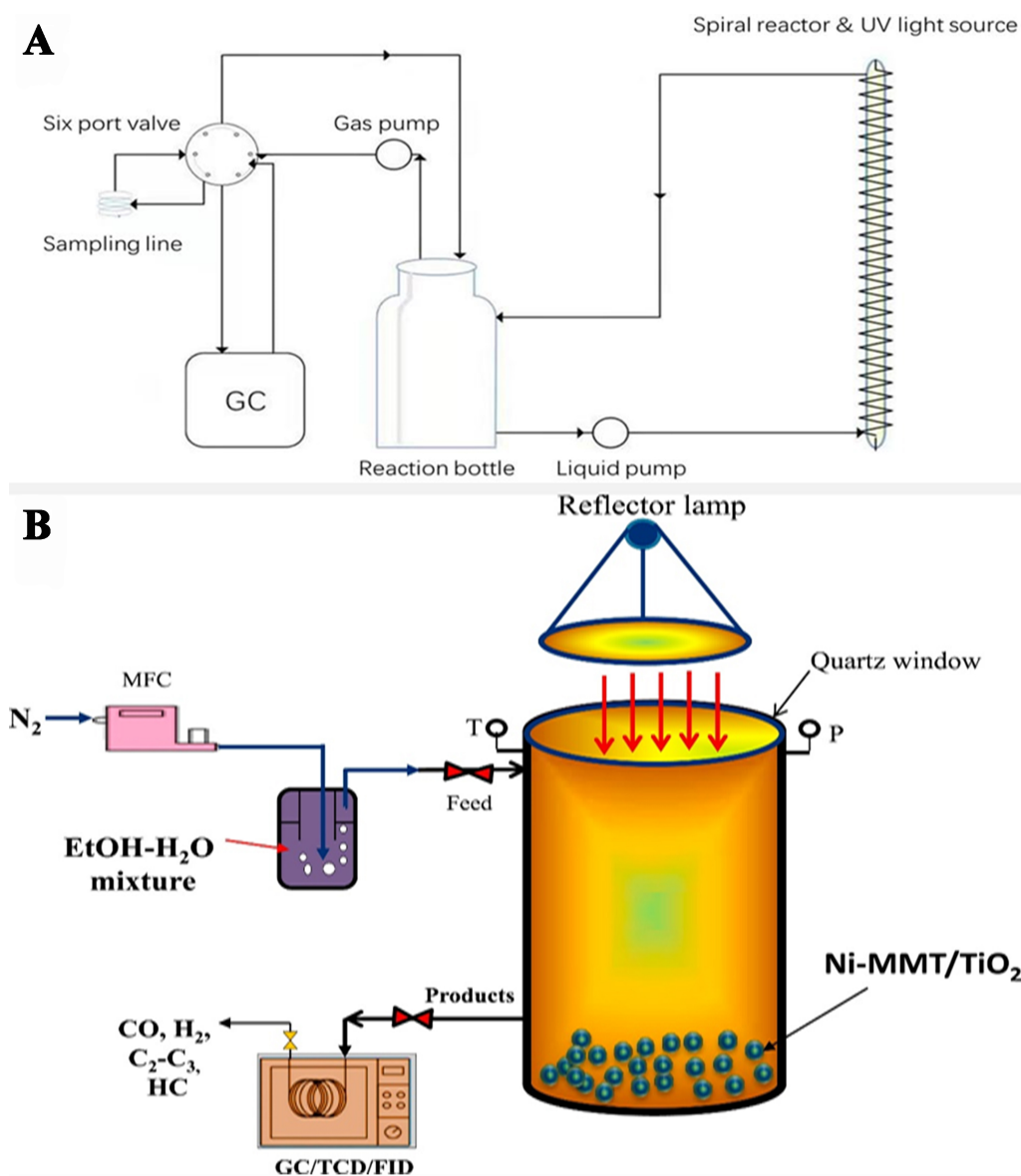


**Figure 16.** (A) Schematic representation of a spiral photoreforming reaction with a reaction bottle, automated gas sampling system, gas pump, liquid pump, and UV fluorescent lamp<sup>[149]</sup>. Copyright 2023, Author(s). Published by Elsevier B.V.; (B) Diagrammatic representation of the experimental setup for a gas-phase photoreactor's photocatalytic  $H_2$  generation from an ethanol-water mixture when exposed to UV light<sup>[150]</sup>. Copyright 2017, Hydrogen Energy Publications LLC. Published by Elsevier Ltd. All rights reserved. UV: Ultraviolet.

over multiple cycles. Based on the experimental results, a reaction mechanism was proposed for the photocatalytic synthesis of  $H_2$  and  $CH_4$  from an ethanol-water mixture in a gas phase system, as depicted in Figure 17A and B. The energy level diagram of Ni-MMT/ $TiO_2$  photocatalysts for  $H_2$  production and the schematic representation of the photocatalytic  $H_2$  and hydrocarbon production over the MMT-Ni/ $TiO_2$  sample, as depicted in Figure 17C and D<sup>[150]</sup>.

Zhang *et al.* synthesized  $TiO_2$ -supported Au catalysts [ $Au@TiO_2$  ( $Ti^{3+}$ )] using the sol-gel method, varying the concentration of the  $NaBH_4$  reducing agent to optimize the production of  $H_2$  and  $CH_4$  through ethanol photoreforming. Increasing the  $NaBH_4$  concentration led to a higher  $Ti^{3+}$  defect concentration, consequently



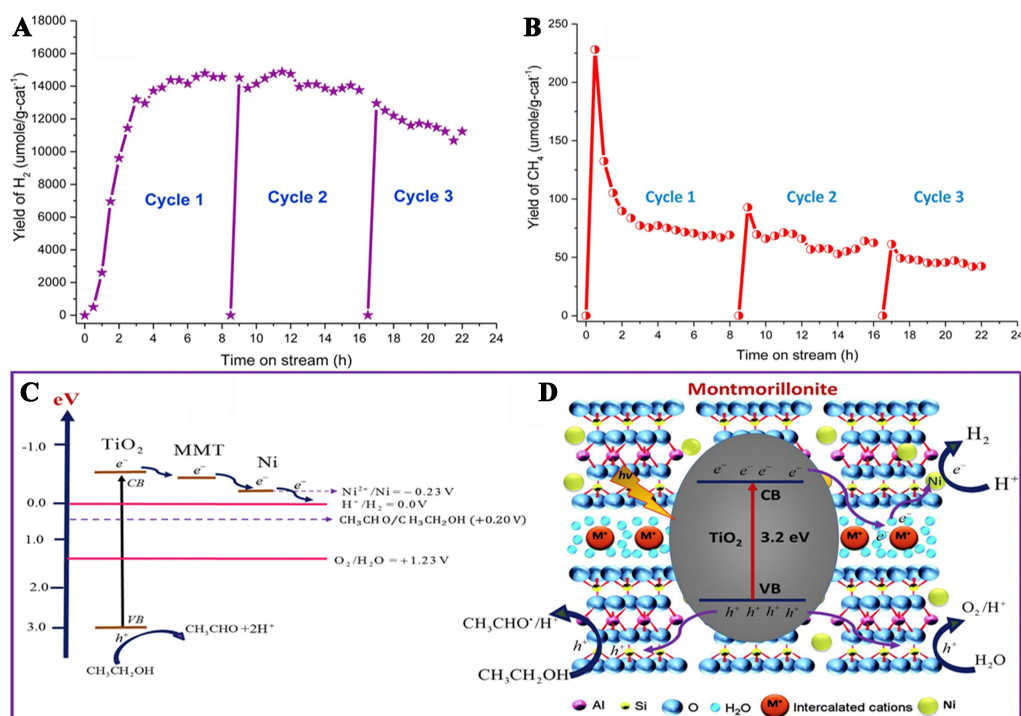


**Figure 17.** (A) Stability analysis of 3% Ni-10% MMT/TiO<sub>2</sub> catalysts for photocatalytic H<sub>2</sub> production and (B) CH<sub>4</sub> production from ethanol-water reforming; (C) Energy level illustration of Ni-MMT/TiO<sub>2</sub> photocatalysts for H<sub>2</sub> production; (D) Schematic representation of photocatalytic H<sub>2</sub> and hydrocarbon production over MMT-Ni/TiO<sub>2</sub> samples<sup>[150]</sup>. Copyright 2017, Hydrogen Energy Publications LLC. Published by Elsevier Ltd. All rights reserved. MMT: Montmorillonite.

boosting the number of oxygen vacancies (V<sub>Os</sub>) and the amount of electron-rich Au in TiO<sub>2</sub>. The catalytic activity of the catalysts improved with concentration of defect sites. The Au@TiO<sub>2</sub> catalyst with the highest defect concentration exhibited exceptional performance during ethanol photoreforming, producing high-quality H<sub>2</sub> at approximately 7,093 μmol·g<sub>cat</sub><sup>-1</sup>·h<sup>-1</sup> and CH<sub>4</sub> via C–C bond cleavage of ethanol, without CO<sub>2</sub> emission. Additionally, the catalyst improved charge carrier generation by enhancing visible light absorption, which accelerated the proton reduction rate to H<sub>2</sub>. The adsorption and activation of ethanol on the catalyst surface further contributed to the improved H<sub>2</sub> production rate, as depicted in Figure 18<sup>[151]</sup>.

Li *et al.* synthesized CdS/metal-organic framework (MOF) composites, specifically CdS/MIL-53(Fe), using the hydrothermal method. These composites demonstrated efficient photocatalytic production of H<sub>2</sub> (2,334 μmol·g<sup>-1</sup>·h<sup>-1</sup>) and benzaldehyde (2,825 μmol·g<sup>-1</sup>·h<sup>-1</sup>) from liquid organic waste under visible light irradiation, achieving a remarkable dual-product outcome from a single reaction. The enhanced photocatalytic activity of CdS/MoF was attributed to increased charge transfer and reduced charge carrier recombination, as evidenced by the photoluminescence (PL), photocurrent, electrochemical impedance spectroscopy (EIS), and Mott-Schottky measurements. A schematic of the photocatalytic efficiency of both H<sub>2</sub> and benzaldehyde production is shown in Figure 19<sup>[152]</sup>.

Jiang *et al.* prepared Co/CdS photocatalysts by using an *in situ* photodeposition method for the simultaneous evolution of hydrogen and benzaldehyde under visible light. The benzaldehyde production yield reached 94.4%. The photocatalytic mechanism highlights the crucial role of benzyl alcohol oxidation in the selective production of benzaldehyde. Notably, the hydrogen evolution via photocatalytic dehydrogenation of benzyl alcohol reached a record-high quantum efficiency, with an average actual



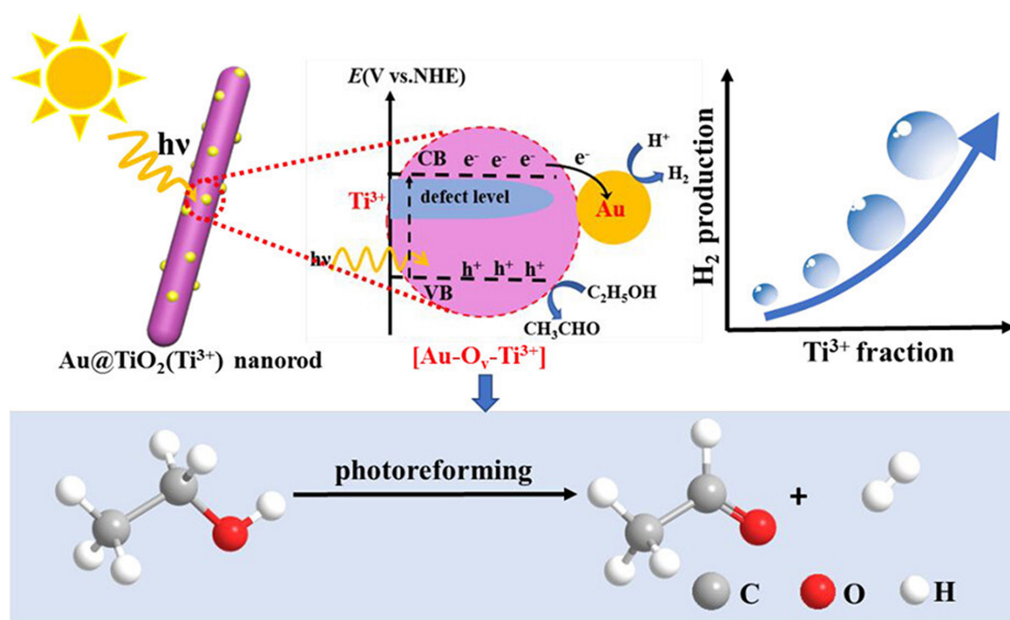


**Figure 18.** The mechanism of ethanol photoreforming by Au@TiO<sub>2</sub> photocatalysts into H<sub>2</sub> and CH<sub>4</sub><sup>[151]</sup>. Copyright 2019, American Chemical Society.

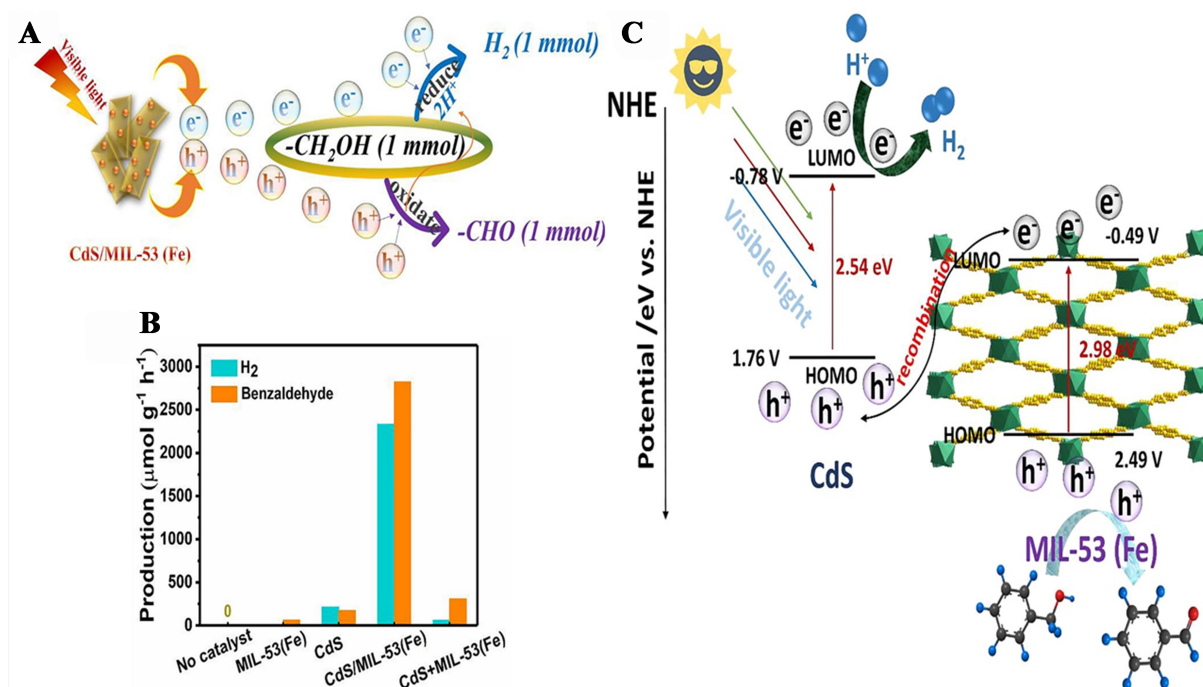


**Figure 19.** (A) Photocatalytic H<sub>2</sub> production and benzaldehyde; (B) Photocatalytic efficiency of dissimilar catalysts with 0.5 mmol benzyl alcohol, CH<sub>3</sub>CN<sub>5</sub> mL, λ > 420 nm; (C) Graphic illustration of CdS/MIL-53(Fe) for the e-h transfer mechanism (Z-scheme)<sup>[152]</sup>. Copyright 2021, Elsevier B.V. All rights reserved.

quantum content of 63.2% at 420 nm in a 50 vol% benzyl alcohol-acetonitrile solution, demonstrating optimal hydrogen evolution performance. This study provides a promising approach for developing highly efficient photosynthesis systems that do not require sacrificial electron donors or noble metal cocatalysts<sup>[153]</sup>.

Tayyab *et al.* synthesized cadmium sulfide nanowires with vanadium carbide as a cocatalyst (VC/CdS) using the calcination method and superficial electrostatic self-assembly. This study demonstrated the use of VC/CdS photocatalysts for the simultaneous production of hydrogen and highly valued organic compounds in a single aqueous system or liquid organic waste. The VC/CS-15 composite exhibited the highest performance, significantly enhancing the selective oxidation of benzyl alcohol to benzaldehyde and simultaneous  $H_2$  generation. Under visible light irradiation ( $\lambda > 420$  nm) for 2 h, the maximum hydrogen evolution rate reached  $20.5 \text{ mmol}\cdot\text{g}^{-1}\cdot\text{h}^{-1}$ , with a selectivity of over 99% for benzaldehyde synthesis. This performance is more than 661 times higher than that of pure CdS nanowires. The enhanced photocatalytic activity is attributed to VC, which lowers the zeta potential, attracts benzyl alcohol, creates active sites for hydrogen generation, and prolongs electron-hole pair separation, thereby increasing the overall efficiency of the photocatalytic process<sup>[154]</sup>.

Zhang *et al.* synthesized silver nanoparticles (AgNPs)/CdS hybrid photocatalysts using a microwave-assisted method followed by the photodeposition method in the presence of methanol under vacuum conditions. The prepared photocatalyst was used to split ethanol into  $H_2$  and acetaldehyde under visible light at room temperature without producing  $CO_x$ . The incorporation of AgNPs enhanced the stability and activity of the photocatalysts, enabling the use of light radiation above 650 nm. This increased electron-hole generation and decrease in charge carrier recombination expands the potential applications of photocatalysis. The AgNPs/CdS hybrid photocatalyst demonstrated over 40 times greater efficiency in ethanol dehydrogenation into  $H_2$  and acetaldehyde than pristine CdS, making it a highly favorable material for low-carbon, green chemistry, and sustainable development<sup>[155]</sup>.

Fu *et al.* synthesized  $ZnSn(OH)_6$  nanocubes (ZHS) using a solvothermal technique to reform an aqueous ethanol solution to  $H_2$  and  $CH_4$ . Various characterization techniques, including transmission electron microscopy, scanning electron microscopy,  $N_2$  sorption [Brunauer–Emmett–Teller (BET) surface area], X-ray diffraction, and UV-visible diffuse reflectance spectroscopy, were utilized to analyze the samples. Among the different samples, the ZHS-20 photocatalysts exhibited the highest photocatalytic activity. However, further enhancement was achieved by loading Pt onto the ZHS-20 surface. The Pt-loaded ZHS-20 catalyst demonstrated superior photocatalytic performance, significantly improving the production of  $H_2$  and  $CH_4$  from the ethanol-water mixture<sup>[156]</sup>.

Li *et al.* fabricated  $Pd/HNb_3O_8-H_2$  photocatalysts using a thermal treatment method involving the integration of  $Pd^{2+}$  into  $HNb_3O_8$  in a  $H_2/Ar$  gas atmosphere. The presence of Pd facilitates the formation of surface  $V_{O_s}$  in  $HNb_3O_8$ , creating dual active sites for the concurrent production of hydrogen and benzaldehyde. The photoelectrochemical and spectroscopy investigations highlight the advantages of the  $Pd/HNb_3O_8-H_2$  photocatalyst in improving the separation and migration of photoinduced charge carriers. This catalyst demonstrated exceptional performance in the co-production of  $H_2$  and benzaldehyde from benzyl-alcohol solutions in water, achieving impressive rates of  $3.17$  and  $2.76 \text{ mmol}\cdot\text{g}^{-1}\cdot\text{h}^{-1}$ , respectively. By integrating experimental data and theoretical studies, the authors investigated the cooperative mechanism between Pd and surface  $V_{O_s}$  on  $HNb_3O_8$ , which significantly enhances the photocatalytic activity for hydrogen evolution coupled with the selective oxidation of benzyl alcohol, as illustrated in Figure 20<sup>[104]</sup>.

Liu *et al.* synthesized a Z-scheme MOF-derived  $Co_9S_8/CdS$  heterostructure using the hydrothermal method for  $H_2$  production and benzaldehyde synthesis. This MOF-derived  $Co_9S_8/CdS$  photocatalyst exhibited superior  $H_2$  production activity, reaching  $61,924 \text{ }\mu\text{mol}\cdot\text{g}^{-1}$  in 6 h and a maximum benzaldehyde output, which was 21 and 16 times greater than that of bare CdS and  $Co_9S_8/CdS$  composite, respectively. Notably, the efficiency of the proposed system surpassed that of most CdS-based photocatalytic systems that rely on

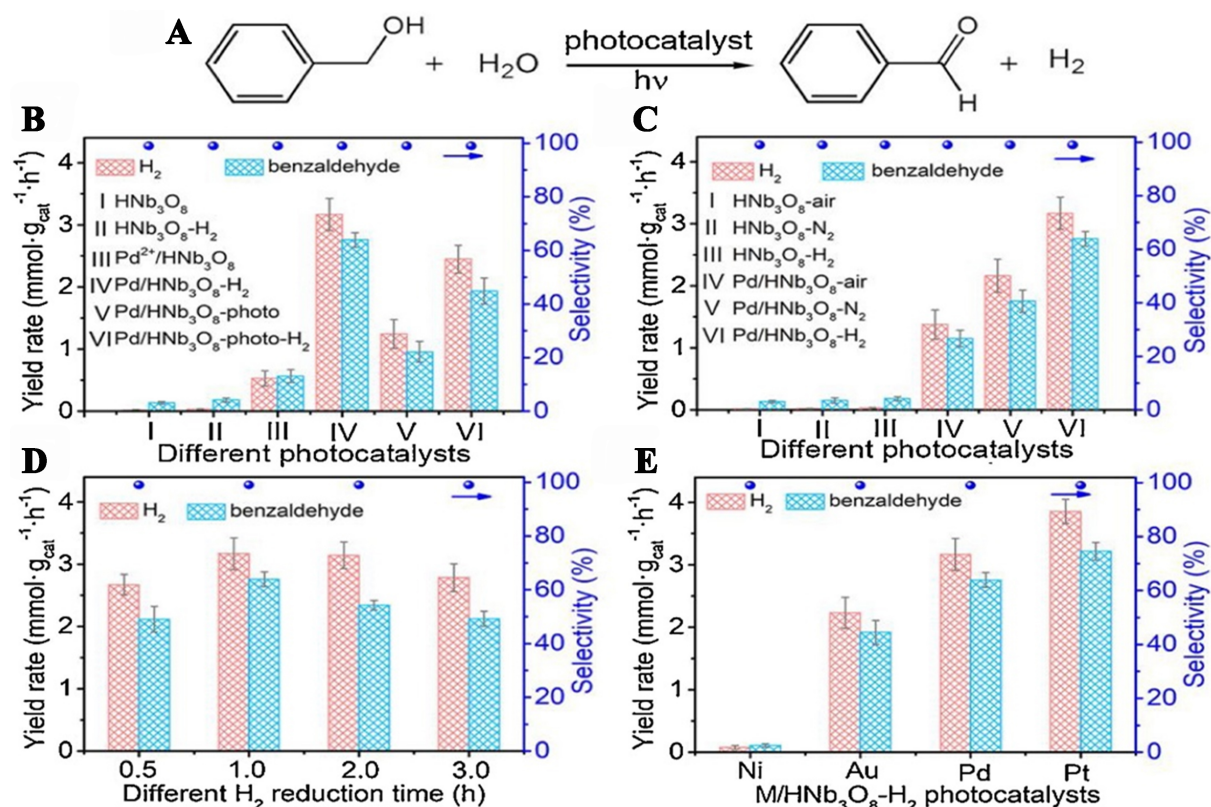


**Figure 20.** (A) Photocatalytic chemical reaction yielding benzaldehyde and H<sub>2</sub> simultaneously. Output rates of benzaldehyde and H<sub>2</sub> over (B) various photocatalysts fabricated by several treatments; (C) photocatalysts through thermal treatment in numerous atmospheres; (D) optimized photocatalysts at different times prepared by thermal treatment; and (E) various M/HNb<sub>3</sub>O<sub>8</sub>-H<sub>2</sub> (M = Pt, Ni, Pd, Au) photocatalysts acquired by thermal treatment<sup>[104]</sup>. Copyright 2021, Elsevier B.V. All rights reserved.

high concentrations of sacrificial agents. This study demonstrated a novel approach to constructing a Z-scheme heterostructure from a multivariate crystalline framework, significantly enhancing the co-production of valuable chemicals such as benzaldehyde and solar fuel without the need for sacrificial agents<sup>[157]</sup>.

Zhang *et al.* fabricated non-metals such as phosphorus (P) and sulfur (S)-doped g-C<sub>3</sub>N<sub>4</sub> hierarchical mesoporous spheres using the co-precipitation method for photocatalytic H<sub>2</sub> and benzaldehyde production. Through experimental analysis and density functional theory (DFT) calculations, the study identified promising doping sites and their positive effects on electronic structure. The optimized S-doped g-C<sub>3</sub>N<sub>4</sub> photocatalysts exhibited a 13.2-fold enhancement in H<sub>2</sub> production compared to bare g-C<sub>3</sub>N<sub>4</sub> under visible light irradiation. Additionally, S-doped g-C<sub>3</sub>N<sub>4</sub> demonstrated outstanding dual-function photocatalytic performance, producing H<sub>2</sub> and benzaldehyde from the oxidation of benzyl alcohol at rates of 3.76 and 3.87 μmol·g<sup>-1</sup>·h<sup>-1</sup>, respectively. This enhanced photocatalytic activity can be attributed to improved charge-carrier separation and transfer capabilities, along with enhanced visible-light absorption<sup>[158]</sup>.

Lin *et al.* prepared nickel-modified ZnIn<sub>2</sub>S<sub>4</sub> (Ni:ZIS) by *in situ* photodeposition treatment for highly efficient photocatalytic H<sub>2</sub> evolution and selective oxidation of benzyl alcohol to benzaldehyde, as illustrated in the schematic mechanism in Figure 21. The incorporation of Ni into ZnIn<sub>2</sub>S<sub>4</sub> facilitates photogenerated charge transfer by promoting α-H abstraction, thereby enhancing H<sub>2</sub> and benzaldehyde photoactivity under visible light irradiation. Further electron paramagnetic resonance (EPR) spectral analysis and quenching

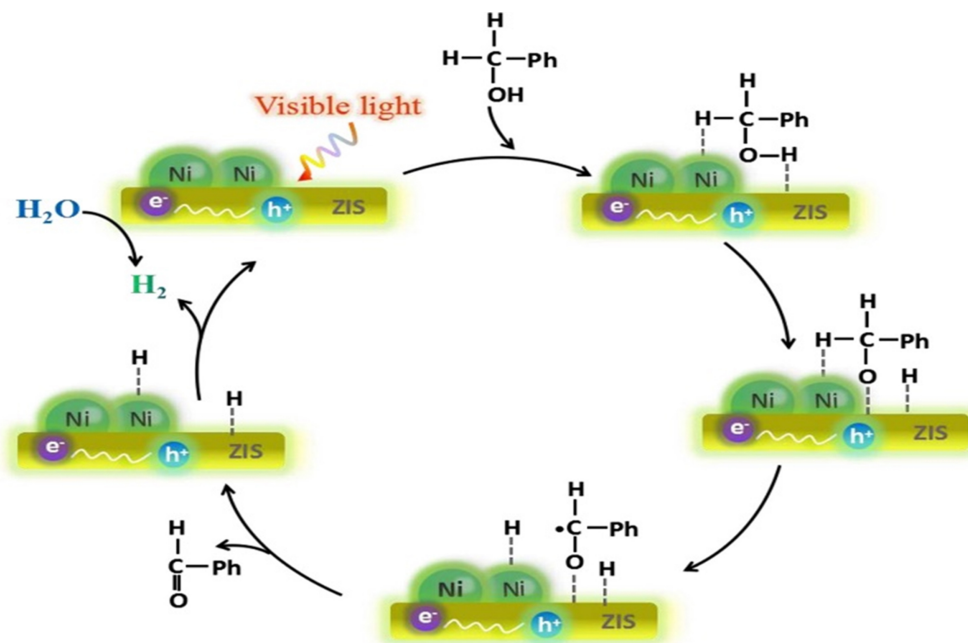


**Figure 21.** Schematic mechanism illustrating the photoredox-catalyzed transformation of benzyl alcohol and the evolution of H<sub>2</sub> over Ni:ZIS in a N<sub>2</sub> atmosphere using visible light ( $\lambda > 420$  nm)<sup>[159]</sup>. Copyright 2020, Elsevier B.V. All rights reserved.

experiments confirmed that a radical mechanism centered on carbon catalyzes the photocatalytic benzyl alcohol conversion activity<sup>[159]</sup>.

Hao *et al.* developed a ZnS/Ni<sub>x</sub>S<sub>y</sub> composite with dual functions for H<sub>2</sub> evolution and benzaldehyde production via the selective oxidation of benzyl alcohols in anaerobic water under UV light. The composite facilitates a transition from hole-predominant oxidation on the ZnS surface to electron-initiating dehydrogenation of alcohols on Ni<sub>x</sub>S<sub>y</sub> nanoparticles. The Ni<sub>x</sub>S<sub>y</sub> nanoparticles exhibit a remarkable ability to abstract H atoms from alcohol and desorb the produced benzaldehyde, as confirmed by hydroxyl radical detection and various active species trapping experiments. In addition, compared with the equivalent acetonitrile system, the ZnS-Ni<sub>x</sub>S<sub>y</sub> composites demonstrated higher conversion efficiency in benzyl alcohol aqueous solution. This study highlights the potential of using Ni<sub>x</sub>S<sub>y</sub> nanoparticles as dehydrogenation units and for hydrogen evolution, thereby improving the performance of wide-band-gap catalysts for discriminating benzyl alcohol transformations coupled with hydrogen evolution in green aqueous solutions<sup>[160]</sup>.

Wang *et al.* fabricated Pd-doped TiO<sub>2</sub> with V<sub>O</sub>s (Pd<sub>SA+C</sub>/TiO<sub>2</sub>-V<sub>O</sub>) using a facile pyrolysis method for the production of H<sub>2</sub> and the oxidation of benzylamine into N-benzylidenebenzylamine. The Pd<sub>SA+C</sub>/TiO<sub>2</sub>-V<sub>O</sub> photocatalyst, which contains Pd single atoms (SAs), clusters (C), and V<sub>O</sub>s, demonstrated superior performance compared with Pd<sub>SA</sub>/TiO<sub>2</sub>-V<sub>O</sub> and TiO<sub>2</sub>-V<sub>O</sub>. The Pd<sub>SA+C</sub>/TiO<sub>2</sub>-V<sub>O</sub> demonstrated remarkable production rates of H<sub>2</sub> and N-benzylidenebenzylamine which were 52.7 and 1.5 times higher, respectively, than TiO<sub>2</sub>-V<sub>O</sub>, as illustrated in Figure 22. Theoretical and experimental studies have elucidated the synergistic mechanism of Pd SAs, clusters, and V<sub>O</sub>s on TiO<sub>2</sub> in enhancing photocatalytic performance. Pd clusters facilitate efficient charge separation and provide optimal active sites for H<sub>2</sub> evolution, whereas Pd SAs contribute to the formation and stabilization of V<sub>O</sub>s through the creation of a Pd + O + Ti<sup>3+</sup> atomic interface<sup>[99]</sup>.



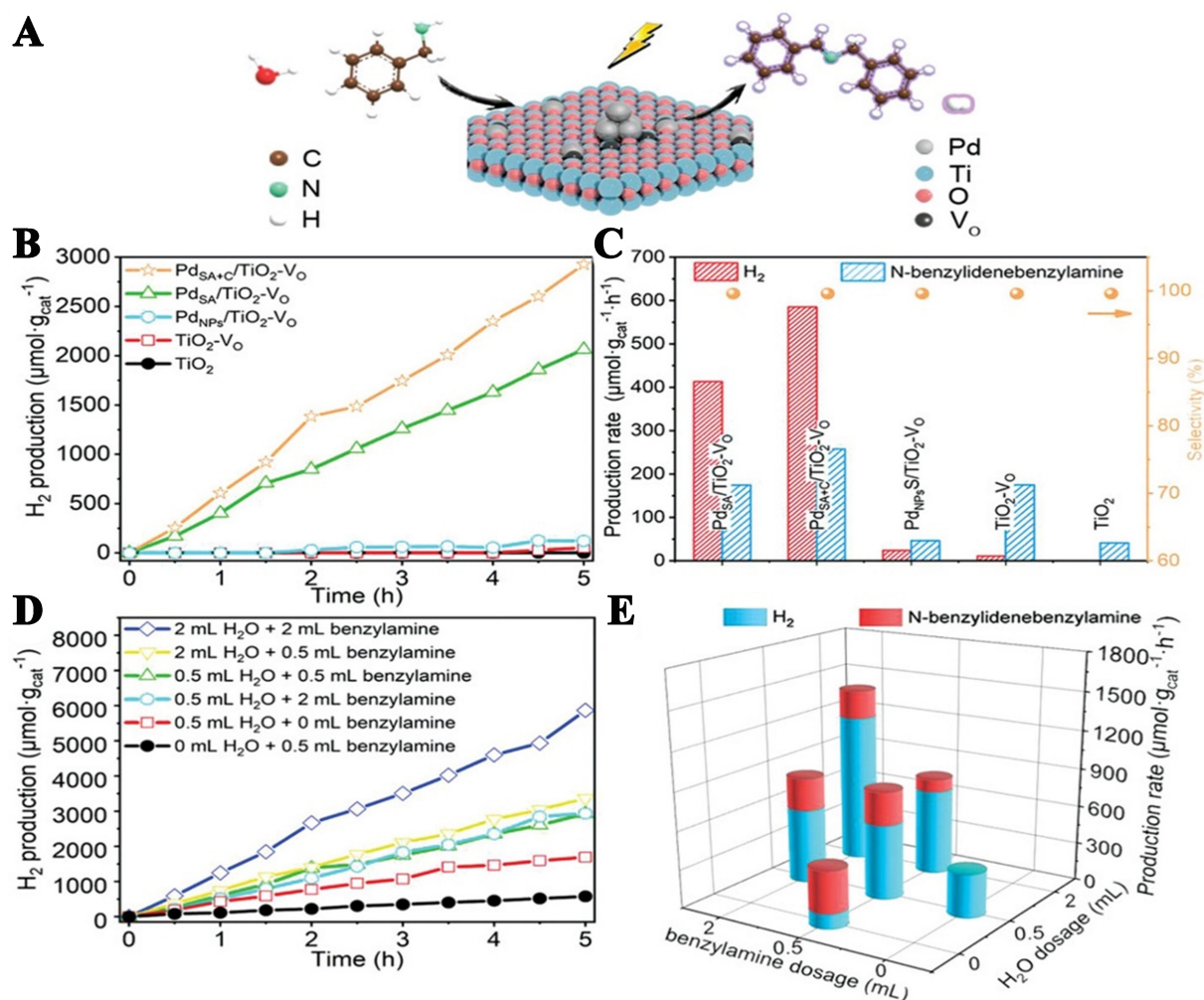


**Figure 22.** Photocatalytic synergistic H<sub>2</sub> production and N-benzylidene benzylamine. (A) Graphical illustration of the photocatalytic reaction; (B) evolution of H<sub>2</sub> using various photocatalysts; (C) different amounts of H<sub>2</sub> and N-benzylidenebenzylamine using various photocatalysts; (D) H<sub>2</sub> evolution with different dosages of H<sub>2</sub>O and benzylamine over Pd<sub>SA+C</sub>/TiO<sub>2</sub>-V<sub>0</sub> photocatalyst; and (E) production rates of N-benzylidenebenzylamine and H<sub>2</sub> over the Pd<sub>SA+C</sub>/TiO<sub>2</sub>-V<sub>0</sub> photocatalyst at varying dosages of H<sub>2</sub>O and benzylamine<sup>[99]</sup>. Copyright 2020, Wiley-VCH GmbH.

Chen *et al.* fabricated MoS<sub>2</sub>/ZnIn<sub>2</sub>S<sub>4</sub> photocatalysts using a facile photochemical reduction method for the conversion of benzyl alcohol into hydrogen and valuable organic compounds such as benzaldehyde under visible light irradiation. The optimized 1%MoS<sub>2</sub>/ZnIn<sub>2</sub>S<sub>4</sub> composite exhibited enhanced visible light absorption and photocatalytic activity, with benzyl alcohol conversion and H<sub>2</sub> evolution rates of 3.69 and 3.88 mmol·g<sup>-1</sup>·h<sup>-1</sup>, respectively, which were six times higher than those of bare ZnIn<sub>2</sub>S<sub>4</sub>. The MoS<sub>2</sub> cocatalyst accelerated the kinetics of H<sub>2</sub> formation for collaborative production reactions by significantly enhancing charge separation and reducing the overpotential of the HER. The molecular suitability of MoS<sub>2</sub> as a high-performance cocatalyst was further confirmed by examining the photoreduction of Cr (VI) and 4-nitroaniline (4-NA). A carbon-centered radical mechanism was identified for the conversion of benzyl alcohol by the MoS<sub>2</sub>/ZnIn<sub>2</sub>S<sub>4</sub> photocatalyst<sup>[86]</sup>.

Qi *et al.* fabricated a CdS/SiO<sub>2</sub> composite using a grinding method by loading CdS quantum dots (QDs) onto spherical SiO<sub>2</sub> to enable H<sub>2</sub> evolution and the dehydrogenative C-C coupling of benzyl alcohol into

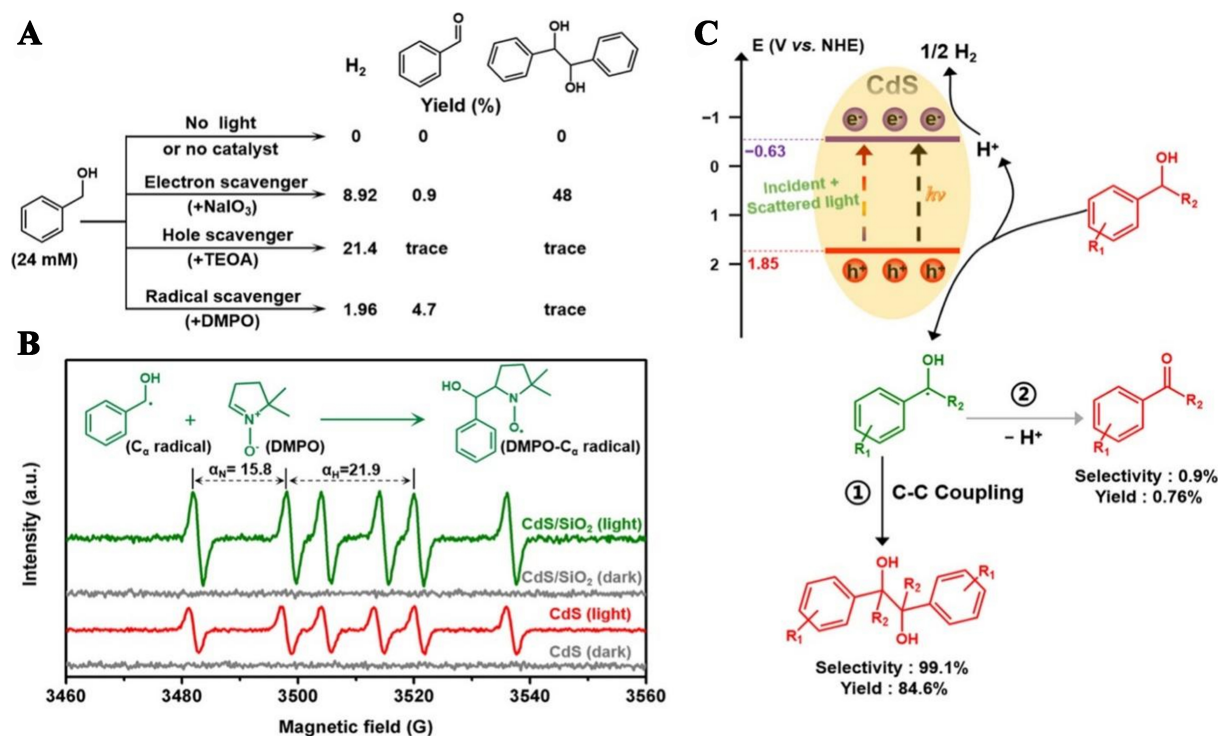


**Figure 23.** (A) Scavenger test experiments of the optimized CdS/SiO<sub>2</sub> photocatalyst with different scavengers at a constant concentration (24 mM) over a 12-h reaction period; (B) *In situ* EPR spectra of CdS and CdS/SiO<sub>2</sub> composites in CH<sub>3</sub>CN solution saturated with argon (Ar) in the presence of a DMPO scavenger; (C) Graphic diagram of simultaneous photocatalytic production of H<sub>2</sub> and hydrobenzoin<sup>[102]</sup>. Copyright 2020, American Chemical Society. EPR: Electron paramagnetic resonance; DMPO: 5, 5-dimethyl-1-pyrroline N-oxide.

hydrobenzoin. The CdS/SiO<sub>2</sub> composite demonstrated enhanced stability and improved photoredox-catalytic activity, effectively facilitating the C-C coupling of benzyl alcohol to form hydrobenzoin and the evolution of H<sub>2</sub>, as depicted in Figure 23A–C<sup>[102]</sup>.

## CONCLUSION

In conclusion, this review provides a comprehensive overview of the latest advancements in photocatalytic hydrogen production and simultaneous chemical synthesis from wastewater or liquid organic waste. The fundamental concepts of cooperative H<sub>2</sub> production and photocatalytic selective organic synthesis were briefly reviewed, followed by an analysis of the critical requirements for semiconductors used in dual-function photocatalysis systems. Subsequently, examples of innovative materials and approaches used in this field to address current challenges and unlock the full potential of nanophotocatalysts were presented. Each example describes the associated photocatalytic reaction or mechanism. There are opportunities and challenges in the advancement of such dual-function photocatalysis. To achieve more effective solar light utilization and synergistic photocatalytic activity, the primary focus of catalyst preparation is the modification of its components and microstructure to improve light absorption, charge separation and migration, and redox capacity of the base catalyst. Adopting a binary analysis perspective, this study focuses on the following key points in order of importance:

- (i) The necessity for dual-directional optimization in photocatalytic hydrogen production with synergistic organic synthesis.
- (ii) The efficiency of photocatalytic hydrogen production is not always compromised by replacing sacrificial agents. Instead, properly integrated organic synthesis from wastewater or liquid organic waste can exert a



multiplier effect.

(iii) The significant potential for advancements and the feasibility analysis of photocatalytic hydrogen production with synergistic organic synthesis.

More effort is required to modify catalysts for hydrogen production and organic synthesis from wastewater or liquid organic waste because this technology remains in its early stages of development and faces significant challenges for broader applications.

## DECLARATIONS

### Acknowledgments

The authors are thankful to the Australian National University (ANU).

### Authors' contributions

Investigation, writing - original draft: Hussain, M. K.

Investigation, analysis: Liu, R.

Analysis: Tanveer, M.; Khalid, N. R.

Conceptualization, supervision: Yin, Z.

### Availability of data and materials

Not applicable.

### Financial support and sponsorship

The authors acknowledge the financial support from the Australian Research Council (FT230100059, DP240100687, IH220100012).

### Conflicts of interest

All authors declared that there are no conflicts of interest.

### Ethical approval and consent to participate

Not applicable.

### Consent for publication

Not applicable.

### Copyright

© The Author(s) 2025.

## REFERENCES

1. Gong, Y.; Wang, J.; Wei, Z.; Zhang, P.; Li, H.; Wang, Y. Combination of carbon nitride and carbon nanotubes: synergistic catalysts for energy conversion. *ChemSusChem* **2014**, *7*, 2303-9. DOI
2. Dai, L.; Chang, D. W.; Baek, J. B.; Lu, W. Carbon nanomaterials for advanced energy conversion and storage. *Small* **2012**, *8*, 1130-66. DOI PubMed
3. George, C.; Ammann, M.; D'Anna, B.; Donaldson, D. J.; Nizkorodov, S. A. Heterogeneous photochemistry in the atmosphere. *Chem. Rev.* **2015**, *115*, 4218-58. DOI PubMed PMC
4. Hussain, M. K.; Khalid, N.; Tanveer, M.; Kebaili, I.; Alrobei, H. Fabrication of CuO/MoO<sub>3</sub> p-n heterojunction for enhanced dyes degradation and hydrogen production from water splitting. *Int. J. Hydrogen. Energy.* **2022**, *47*, 15491-504. DOI
5. Bard, A. J.; Fox, M. A. Artificial photosynthesis: solar splitting of water to hydrogen and oxygen. *Acc. Chem. Res.* **1995**, *28*, 141-5. DOI
6. Yang, J.; Wang, D.; Han, H.; Li, C. Roles of cocatalysts in photocatalysis and photoelectrocatalysis. *Acc. Chem. Res.* **2013**, *46*, 1900-9. DOI

7. Tu, W.; Zhou, Y.; Zou, Z. Versatile graphene-promoting photocatalytic performance of semiconductors: basic principles, synthesis, solar energy conversion, and environmental applications. *Adv. Funct. Mater.* **2013**, *23*, 4996-5008. DOI
8. Fan, W.; Zhang, Q.; Wang, Y. Semiconductor-based nanocomposites for photocatalytic H<sub>2</sub> production and CO<sub>2</sub> conversion. *Phys. Chem. Chem. Phys.* **2013**, *15*, 2632-49. DOI
9. Wondraczek, L.; Tyystjärvi, E.; Méndez-Ramos, J.; Müller, F. A.; Zhang, Q. Shifting the sun: solar spectral conversion and extrinsic sensitization in natural and artificial photosynthesis. *Adv. Sci.* **2015**, *2*, 1500218. DOI PubMed PMC
10. Kapilashrami, M.; Zhang, Y.; Liu, Y. S.; Hagfeldt, A.; Guo, J. Probing the optical property and electronic structure of TiO<sub>2</sub> nanomaterials for renewable energy applications. *Chem. Rev.* **2014**, *114*, 9662-707. DOI PubMed
11. Kubacka, A.; Fernández-García, M.; Colón, G. Advanced nanoarchitectures for solar photocatalytic applications. *Chem. Rev.* **2012**, *112*, 1555-614. DOI PubMed
12. Pan, J.; Wang, B.; Shen, S.; Chen, L.; Yin, S. Introducing bidirectional axial coordination into BiVO<sub>4</sub>@metal phthalocyanine core-shell photoanodes for efficient water oxidation. *Angew. Chem. Int. Ed. Engl.* **2023**, *135*, e202307246. DOI
13. Li, H.; Zhou, Y.; Tu, W.; Ye, J.; Zou, Z. State-of-the-art progress in diverse heterostructured photocatalysts toward promoting photocatalytic performance. *Adv. Funct. Mater.* **2015**, *25*, 998-1013. DOI
14. Zhang, H.; Liu, G.; Shi, L.; Liu, H.; Wang, T.; Ye, J. Engineering coordination polymers for photocatalysis. *Nano. Energy.* **2016**, *22*, 149-68. DOI
15. Hussain, M. K.; Khalid, N.; Tanveer, M.; et al. In-situ fabrication of MoO<sub>3</sub> hexagonal flowers decorated with Co<sub>3</sub>O<sub>4</sub> microrods with enhanced photocatalytic activity and stability under visible light irradiation. *Mater. Chem. Phys.* **2023**, *302*, 127652. DOI
16. Chen, G.; Waterhouse, G. I. N.; Shi, R.; et al. From solar energy to fuels: recent advances in light-driven C<sub>1</sub> chemistry. *Angew. Chem. Int. Ed. Engl.* **2019**, *58*, 17528-51. DOI
17. Mustafa, A.; Lougou, B. G.; Shuai, Y.; Wang, Z.; Tan, H. Current technology development for CO<sub>2</sub> utilization into solar fuels and chemicals: a review. *J. Energy. Chem.* **2020**, *49*, 96-123. DOI
18. Qi, J.; Zhang, W.; Cao, R. Solar-to-hydrogen energy conversion based on water splitting. *Adv. Energy. Mater.* **2018**, *8*, 1701620. DOI
19. Aslam, U.; Rao, V. G.; Chavez, S.; Linic, S. Catalytic conversion of solar to chemical energy on plasmonic metal nanostructures. *Nat. Catal.* **2018**, *1*, 656-65. DOI
20. Wang, Q.; Pornrungraj, C.; Linley, S.; Reisner, E. Strategies to improve light utilization in solar fuel synthesis. *Nat. Energy.* **2022**, *7*, 13-24. DOI
21. Agosti, A.; Nakibli, Y.; Amirav, L.; Bergamini, G. Photosynthetic H<sub>2</sub> generation and organic transformations with CdSe@CdS-Pt nanorods for highly efficient solar-to-chemical energy conversion. *Nano. Energy.* **2020**, *70*, 104510. DOI
22. Xu, X.; Su, C.; Shao, Z. Fundamental understanding and application of Ba<sub>0.5</sub>Sr<sub>0.5</sub>Co<sub>0.8</sub>Fe<sub>0.2</sub>O<sub>3-δ</sub> perovskite in energy storage and conversion: past, present, and future. *Energy. Fuels.* **2021**, *35*, 13585-609. DOI
23. Zhou, B.; Zhou, P.; Dong, W.; Mi, Z. Gallium nitride-based artificial photosynthesis integrated devices for solar hydrogen generation and carbon dioxide reduction. In: Varghese OK, Souza FL, editors. Conversion of water and CO<sub>2</sub> to fuels using solar energy. Wiley; 2024. pp. 309-39. DOI
24. Qi, M. Y.; Conte, M.; Anpo, M.; Tang, Z. R.; Xu, Y. J. Cooperative coupling of oxidative organic synthesis and hydrogen production over semiconductor-based photocatalysts. *Chem. Rev.* **2021**, *121*, 13051-85. DOI PubMed
25. Franchi, D.; Amara, Z. Applications of sensitized semiconductors as heterogeneous visible-light photocatalysts in organic synthesis. *ACS. Sustainable. Chem. Eng.* **2020**, *8*, 15405-29. DOI
26. Gisbertz, S.; Pieber, B. Heterogeneous photocatalysis in organic synthesis. *ChemPhotoChem* **2020**, *4*, 456-75. DOI
27. Molinari, R.; Lavorato, C.; Argurio, P. Recent progress of photocatalytic membrane reactors in water treatment and in synthesis of organic compounds. a review. *Catal. Today.* **2017**, *281*, 144-64. DOI
28. Friedmann, D.; Hakki, A.; Kim, H.; Choi, W.; Bahnemann, D. Heterogeneous photocatalytic organic synthesis: state-of-the-art and future perspectives. *Green. Chem.* **2016**, *18*, 5391-411. DOI
29. Dai, X.; Xie, M.; Meng, S.; Fu, X.; Chen, S. Coupled systems for selective oxidation of aromatic alcohols to aldehydes and reduction of nitrobenzene into aniline using CdS/g-C<sub>3</sub>N<sub>4</sub> photocatalyst under visible light irradiation. *Appl. Catal. B. Environ.* **2014**, *158-9*, 382-90. DOI
30. Huang, H.; Jin, Y.; Chai, Z.; et al. Surface charge-induced activation of Ni-loaded CdS for efficient and robust photocatalytic dehydrogenation of methanol. *Appl. Catal. B. Environ.* **2019**, *257*, 117869. DOI
31. Bie, C.; Wang, L.; Yu, J. Challenges for photocatalytic overall water splitting. *Chem* **2022**, *8*, 1567-74. DOI
32. Rahman, M. Z.; Raziq, F.; Zhang, H.; Gascon, J. Key strategies for enhancing H<sub>2</sub> production in transition metal oxide based photocatalysts. *Angew. Chem. Int. Ed. Engl.* **2023**, *135*, e202305385. DOI PubMed
33. Nishioka, S.; Osterloh, F. E.; Wang, X.; Mallouk, T. E.; Maeda, K. Photocatalytic water splitting. *Nat. Rev. Methods. Primers.* **2023**, *3*, 226. DOI
34. Ismael, M. A review and recent advances in solar-to-hydrogen energy conversion based on photocatalytic water splitting over doped-TiO<sub>2</sub> nanoparticles. *Solar. Energy.* **2020**, *211*, 522-46. DOI
35. Wang, Z.; Li, C.; Domen, K. Recent developments in heterogeneous photocatalysts for solar-driven overall water splitting. *Chem. Soc. Rev.* **2019**, *48*, 2109-25. DOI
36. Miseki, Y.; Sayama, K. Photocatalytic water splitting for solar hydrogen production using the carbonate effect and the Z-scheme

- reaction. *Adv. Energy. Mater.* **2019**, *9*, 1801294. DOI
37. Wang, Y.; Silveri, F.; Bayazit, M. K.; et al. Bandgap engineering of organic semiconductors for highly efficient photocatalytic water splitting. *Adv. Energy. Mater.* **2018**, *8*, 1801084. DOI
38. Maeda, K.; Teramura, K.; Lu, D.; et al. Photocatalyst releasing hydrogen from water. *Nature* **2006**, *440*, 295. DOI
39. Yuan, Y. J.; Lu, H. W.; Yu, Z. T.; Zou, Z. G. Noble-metal-free molybdenum disulfide cocatalyst for photocatalytic hydrogen production. *ChemSusChem* **2015**, *8*, 4113-27. DOI PubMed
40. Moniz, S. J. A.; Shevlin, S. A.; Martin, D. J.; Guo, Z.; Tang, J. Visible-light driven heterojunction photocatalysts for water splitting - a critical review. *Energy. Environ. Sci.* **2015**, *8*, 731-59. DOI
41. Lu, Q.; Yu, Y.; Ma, Q.; Chen, B.; Zhang, H. 2D transition-metal-dichalcogenide-nanosheet-based composites for photocatalytic and electrocatalytic hydrogen evolution reactions. *Adv. Mater.* **2016**, *28*, 1917-33. DOI
42. Zhang, N.; Qu, Y.; Pan, K.; Wang, G.; Li, Y. Synthesis of pure phase  $\text{Mg}_{1.2}\text{Ti}_{1.8}\text{O}_5$  and  $\text{MgTiO}_3$  nanocrystals for photocatalytic hydrogen production. *Nano. Res.* **2016**, *9*, 726-34. DOI
43. Fujishima, A.; Honda, K. Electrochemical photolysis of water at a semiconductor electrode. *Nature* **1972**, *238*, 37-8. DOI
44. Yang, X.; Singh, D.; Ahuja, R. Recent advancements and future prospects in ultrathin 2D semiconductor-based photocatalysts for water splitting. *Catalysts* **2020**, *10*, 1111. DOI
45. Zhong, S.; Xi, Y.; Wu, S.; Liu, Q.; Zhao, L.; Bai, S. Hybrid cocatalysts in semiconductor-based photocatalysis and photoelectrocatalysis. *J. Mater. Chem. A* **2020**, *8*, 14863-94. DOI
46. Zhang, Y.; Xia, B.; Ran, J.; Davey, K.; Qiao, S. Z. Atomic-level reactive sites for semiconductor-based photocatalytic  $\text{CO}_2$  reduction. *Adv. Energy. Mater.* **2020**, *10*, 1903879. DOI
47. Chen, S.; Huang, D.; Xu, P.; et al. Semiconductor-based photocatalysts for photocatalytic and photoelectrochemical water splitting: will we stop with photocorrosion? *J. Mater. Chem. A* **2020**, *8*, 2286-322. DOI
48. Tahir, M.; Asiri, A. M.; Nawaz, T. A perspective on the fabrication of heterogeneous photocatalysts for enhanced hydrogen production. *Int. J. Hydrogen. Energy* **2020**, *45*, 24544-57. DOI
49. Wang, L.; Sasaki, T. Titanium oxide nanosheets: graphene analogues with versatile functionalities. *Chem. Rev.* **2014**, *114*, 9455-86. DOI PubMed
50. Bai, S.; Jiang, W.; Li, Z.; Xiong, Y. Surface and interface engineering in photocatalysis. *ChemNanoMat* **2015**, *1*, 223-39. DOI
51. Martin, D. J.; Liu, G.; Moniz, S. J.; et al. Efficient visible driven photocatalyst, silver phosphate: performance, understanding and perspective. *Chem. Soc. Rev.* **2015**, *44*, 7808-28. DOI
52. Alam, M.; Azam, H.; Khalid, N.; et al. Enhanced photocatalytic performance of  $\text{Ag}_3\text{PO}_4/\text{Mn-ZnO}$  nanocomposite for the degradation of tetracycline hydrochloride. *Crystals* **2022**, *12*, 1156. DOI
53. Hussain, M. K.; Khalid, N.; Tanveer, M.; et al. Facile fabrication of Z-scheme  $\text{ZnO}/\text{MoO}_3$  heterojunction as an excellent visible-light responsive photocatalyst for the degradation of rhodamine B and alizarin yellow dyes. *Opt. Mater.* **2024**, *148*, 114794. DOI
54. Khalid, N.; Hammad, A.; Tahir, M.; et al. Enhanced photocatalytic activity of Al and Fe co-doped  $\text{ZnO}$  nanorods for methylene blue degradation. *Ceram. Int.* **2019**, *45*, 21430-5. DOI
55. Khalid, N. R.; Hussain, M. K.; Murtaza, G.; Ikram, M.; Ahmad, M.; Hammad, A. A novel  $\text{Ag}_2\text{O}/\text{Fe-TiO}_2$  photocatalyst for  $\text{CO}_2$  conversion into methane under visible light. *J. Inorg. Organomet. Polym.* **2019**, *29*, 1288-96. DOI
56. Banisharif, A.; Khodadadi, A. A.; Mortazavi, Y.; et al. Highly active  $\text{Fe}_2\text{O}_3$ -doped  $\text{TiO}_2$  photocatalyst for degradation of trichloroethylene in air under UV and visible light irradiation: experimental and computational studies. *Appl. Catal. B. Environ.* **2015**, *165*, 209-21. DOI
57. Hussain, M. K.; Khalid, N.; Tahir, M.; Tanveer, M.; Iqbal, T.; Liaqat, M. Enhanced visible light-driven photocatalytic activity and stability of novel ternary  $\text{ZnO}/\text{CuO}/\text{MoO}_3$  nanorods for the degradation of rhodamine B and alizarin yellow. *Mater. Sci. Semicond. Process.* **2023**, *155*, 107261. DOI
58. Zhu, D.; Zhou, Q. Novel  $\text{Bi}_2\text{WO}_6$  modified by N-doped graphitic carbon nitride photocatalyst for efficient photocatalytic degradation of phenol under visible light. *Appl. Catal. B. Environ.* **2020**, *268*, 118426. DOI
59. He, W.; Sun, Y.; Jiang, G.; Huang, H.; Zhang, X.; Dong, F. Activation of amorphous  $\text{Bi}_2\text{WO}_6$  with synchronous Bi metal and  $\text{Bi}_2\text{O}_3$  coupling: photocatalysis mechanism and reaction pathway. *Appl. Catal. B. Environ.* **2018**, *232*, 340-7. DOI
60. Tanveer, M.; Cheema, H. H.; Nabi, G.; Ali, A. R.; Hussain, M. K.; Qadeer, M. A novel composite ( $\text{BiVO}_4/\text{TiS}_2$ ) presenting an excellent Z-scheme photocatalytic degradation for Rhodamine B dye under the visible light irradiation. *J. Lumin.* **2024**, *271*, 120585. DOI
61. Tayebi, M.; Lee, B. Recent advances in  $\text{BiVO}_4$  semiconductor materials for hydrogen production using photoelectrochemical water splitting. *Renew. Sustain. Energy. Rev.* **2019**, *111*, 332-43. DOI
62. Gurylev, V. A review on the development and advancement of  $\text{Ta}_2\text{O}_5$  as a promising photocatalyst. *Mater. Today. Sustain.* **2022**, *18*, 100131. DOI
63. Liu, W.; Liao, M.; Huang, S.; Reyes, Y. I. A.; Tiffany, C. H.; Perng, T. Formation and characterization of gray  $\text{Ta}_2\text{O}_5$  and its enhanced photocatalytic hydrogen generation activity. *Int. J. Hydrogen. Energy* **2020**, *45*, 16560-8. DOI
64. Arunachalam, P.; Nagai, K.; Amer, M. S.; Ghanem, M. A.; Ramalingam, R. J.; Al-Mayouf, A. M. Recent developments in the use of heterogeneous semiconductor photocatalyst based materials for a visible-light-induced water-splitting system - a brief review. *Catalysts* **2021**, *11*, 160. DOI
65. Qadeer M, Khalid Hussain M, Tanveer M, Munawar S, Nabi G, Henaish A. Sol-gel extended hydrothermal synthesis of  $\text{BiFeO}_3$

- nano-beads for excellent photocatalytic and photo-electrochemical properties under natural light irradiation. *Inorg. Chem. Commun.* **2023**, *158*, 111617. DOI
66. Zhao, Y.; Liu, W.; Liu, P.; et al. In situ photodeposition of Au nanoparticle plasma: enhanced defect-state g-C<sub>3</sub>N<sub>4</sub> photocatalytic hydrogen evolution. *Cryst. Growth. Des.* **2024**, *24*, 5794-805. DOI
67. Cheng, L.; Xiang, Q.; Liao, Y.; Zhang, H. CdS-based photocatalysts. *Energy. Environ. Sci.* **2018**, *11*, 1362-91. DOI
68. Sun, Y.; Cheng, H.; Gao, S.; et al. Freestanding tin disulfide single-layers realizing efficient visible-light water splitting. *Angew. Chem. Int. Ed. Engl.* **2012**, *124*, 8857-61. DOI
69. Wang, B.; Wang, Y.; Lei, Y.; et al. Mesoporous silicon carbide nanofibers with in situ embedded carbon for co-catalyst free photocatalytic hydrogen production. *Nano. Res.* **2016**, *9*, 886-98. DOI
70. Li, B.; Hu, Y.; Shen, Z.; et al. Photocatalysis driven by near-infrared light: materials design and engineering for environmentally friendly photoreactions. *ACS. EST. Eng.* **2021**, *1*, 947-64. DOI
71. Tan, L.; Ong, W.; Chai, S.; Goh, B. T.; Mohamed, A. R. Visible-light-active oxygen-rich TiO<sub>2</sub> decorated 2D graphene oxide with enhanced photocatalytic activity toward carbon dioxide reduction. *Appl. Catal. B. Environ.* **2015**, *179*, 160-70. DOI
72. Tan, L.; Ong, W.; Chai, S.; Mohamed, A. R. Visible-light-activated oxygen-rich TiO<sub>2</sub> as next generation photocatalyst: importance of annealing temperature on the photoactivity toward reduction of carbon dioxide. *Chem. Eng. J.* **2016**, *283*, 1254-63. DOI
73. Rashid, R.; Shafiq, I.; Gilani, M. R. H. S.; et al. Advancements in TiO<sub>2</sub>-based photocatalysis for environmental remediation: strategies for enhancing visible-light-driven activity. *Chemosphere* **2024**, *349*, 140703. DOI
74. Jiang, A.; Guo, H.; Yu, S.; et al. Dual charge-accepting engineering modified AgIn<sub>5</sub>S<sub>8</sub>/CdS quantum dots for efficient photocatalytic hydrogen evolution overall H<sub>2</sub>S splitting. *Appl. Catal. B. Environ.* **2023**, *332*, 122747. DOI
75. Jeon, T. H.; Koo, M. S.; Kim, H.; Choi, W. Dual-functional photocatalytic and photoelectrocatalytic systems for energy- and resource-recovering water treatment. *ACS. Catal.* **2018**, *8*, 11542-63. DOI
76. He, Y.; Wang, D. Toward practical solar hydrogen production. *Chem* **2018**, *4*, 405-8. DOI
77. Dashtian, K.; Shahsavari, S.; Usman, M.; et al. A comprehensive review on advances in polyoxometalate based materials for electrochemical water splitting. *Coord. Chem. Rev.* **2024**, *504*, 215644. DOI
78. Kampouri, S.; Stylianou, K. C. Dual-functional photocatalysis for simultaneous hydrogen production and oxidation of organic substances. *ACS. Catal.* **2019**, *9*, 4247-70. DOI
79. Sun, W.; Zheng, Y.; Zhu, J. A "win-win" photocatalysis: coupling hydrogen production with the synthesis of high value-added organic chemicals. *Mater. Today. Sustain.* **2023**, *23*, 100465. DOI
80. Schrauzer, G. N.; Guth, T. D. Photolysis of water and photoreduction of nitrogen on titanium dioxide. *J. Am. Chem. Soc.* **1977**, *99*, 7189-93. DOI
81. Mills, A.; Le, H. S. An overview of semiconductor photocatalysis. *J. Photochem. Photobiol. A. Chem.* **1997**, *108*, 1-35. DOI
82. Kampouri, S.; Ireland, C. P.; Valizadeh, B.; et al. Mixed-phase MOF-derived titanium dioxide for photocatalytic hydrogen evolution: the impact of the templated morphology. *ACS. Appl. Energy. Mater.* **2018**, *1*, 6541-8. DOI
83. Wang, Q.; Domen, K. Particulate photocatalysts for light-driven water splitting: mechanisms, challenges, and design strategies. *Chem. Rev.* **2020**, *120*, 919-85. DOI PubMed
84. Xie, S.; Shen, Z.; Deng, J.; et al. Visible light-driven C-H activation and C-C coupling of methanol into ethylene glycol. *Nat. Commun.* **2018**, *9*, 1181. DOI PubMed PMC
85. Chen, S.; Takata, T.; Domen, K. Particulate photocatalysts for overall water splitting. *Nat. Rev. Mater.* **2017**, *2*, 17050. DOI
86. Chen, Z. H.; Li, Y. H.; Qi, M. Y.; Tang, Z. R.; Xu, Y. J. Benzyl alcohol oxidation and hydrogen generation over MoS<sub>2</sub>/ZnIn<sub>2</sub>S<sub>4</sub> composite photocatalyst. *Res. Chem. Intermed.* **2022**, *48*, 1-12. DOI
87. Liu, H.; Xu, C.; Li, D.; Jiang, H. Photocatalytic hydrogen production coupled with selective benzylamine oxidation over MOF composites. *Angew. Chem. Int. Ed. Engl.* **2018**, *130*, 5477-81. DOI
88. Luo, N.; Montini, T.; Zhang, J.; et al. Visible-light-driven coproduction of diesel precursors and hydrogen from lignocellulose-derived methylfurans. *Nat. Energy.* **2019**, *4*, 575-84. DOI
89. Zhang, X.; Liu, T.; Zhao, F.; Zhang, N.; Wang, Y. In-situ-formed Cd and Ag<sub>2</sub>S decorated CdS photocatalyst with boosted charge carrier spatial separation for enhancing UV-vis-NIR photocatalytic hydrogen evolution. *Appl. Catal. B. Environ.* **2021**, *298*, 120620. DOI
90. Naseri, A.; Asghari, S. G.; Samadi, M.; Yousefi, M.; Ebrahimi, M.; Moshfegh, A. Z. Recent advances on dual-functional photocatalytic systems for combined removal of hazardous water pollutants and energy generation. *Res. Chem. Intermed.* **2022**, *48*, 911-33. DOI
91. Zhu, T.; Ye, X.; Zhang, Q.; Hui, Z.; Wang, X.; Chen, S. Efficient utilization of photogenerated electrons and holes for photocatalytic redox reactions using visible light-driven Au/ZnIn<sub>2</sub>S<sub>4</sub> hybrid. *J. Hazard. Mater.* **2019**, *367*, 277-85. DOI
92. Zhang, S.; Wang, K.; Li, F.; Ho, S. Structure-mechanism relationship for enhancing photocatalytic H<sub>2</sub> production. *Int. J. Hydrogen. Energy.* **2022**, *47*, 37517-30. DOI
93. Chen, X.; Shen, S.; Guo, L.; Mao, S. S. Semiconductor-based photocatalytic hydrogen generation. *Chem. Rev.* **2010**, *110*, 6503-70. DOI
94. Rahman, M. Z.; Edvinsson, T.; Gascon, J. Hole utilization in solar hydrogen production. *Nat. Rev. Chem.* **2022**, *6*, 243-58. DOI PubMed
95. Ran, J.; Zhang, J.; Yu, J.; Jaroniec, M.; Qiao, S. Z. Earth-abundant cocatalysts for semiconductor-based photocatalytic water splitting.

- Chem. Soc. Rev. 2014, 43, 7787-812. DOI
96. Zhou, P.; Navid, I. A.; Ma, Y.; et al. Solar-to-hydrogen efficiency of more than 9% in photocatalytic water splitting. *Nature* 2023, 613, 66-70. DOI
97. Liu, S.; Lin, P.; Wu, M.; et al. Organic dyes with multi-branched structures for highly efficient photocatalytic hydrogen evolution under visible-light irradiation. *Appl. Catal. B. Environ.* 2022, 309, 121257. DOI
98. Yang, Y.; Tan, H.; Cheng, B.; Fan, J.; Yu, J.; Ho, W. Near-infrared-responsive photocatalysts. *Small. Methods*. 2021, 5, e2001042. DOI
99. Wang, T.; Tao, X.; Li, X.; Zhang, K.; Liu, S.; Li, B. Synergistic Pd single atoms, clusters, and oxygen vacancies on TiO<sub>2</sub> for photocatalytic hydrogen evolution coupled with selective organic oxidation. *Small* 2021, 17, e2006255. DOI
100. Rusinque, B.; Escobedo, S.; de, L. H. Hydrogen production via Pd-TiO<sub>2</sub> photocatalytic water splitting under near-UV and visible light: analysis of the reaction mechanism. *Catalysts* 2021, 11, 405. DOI
101. Lyubina, T. P.; Markovskaya, D. V.; Kozlova, E. A.; Parmon, V. N. Photocatalytic hydrogen evolution from aqueous solutions of glycerol under visible light irradiation. *Int. J. Hydrogen. Energy*. 2013, 38, 14172-9. DOI
102. Qi, M.; Li, Y.; Anpo, M.; Tang, Z.; Xu, Y. Efficient photoredox-mediated C-C coupling organic synthesis and hydrogen production over engineered semiconductor quantum dots. *ACS. Catal.* 2020, 10, 14327-35. DOI
103. Jia, Q.; Zhang, S.; Jia, X.; Dong, X.; Gao, Z.; Gu, Q. Photocatalytic coupled redox cycle for two organic transformations over Pd/carbon nitride composites. *Catal. Sci. Technol.* 2019, 9, 5077-89. DOI
104. Li, X.; Wang, T.; Zheng, Z.; Yang, Q.; Li, C.; Li, B. Pd modified defective HNb<sub>3</sub>O<sub>8</sub> with dual active sites for photocatalytic coproduction of hydrogen fuel and value-added chemicals. *Appl. Catal. B. Environ.* 2021, 296, 120381. DOI
105. Pomilla, F.; García-lópez, E.; Marci, G.; Palmisano, L.; Parrino, F. Heterogeneous photocatalytic materials for sustainable formation of high-value chemicals in green solvents. *Mater. Today. Sustain.* 2021, 13, 100071. DOI
106. Changotra, R.; Ray, A. K.; He, Q. Establishing a water-to-energy platform via dual-functional photocatalytic and photoelectrocatalytic systems: a comparative and perspective review. *Adv. Colloid. Interface. Sci.* 2022, 309, 102793. DOI PubMed
107. Liu, J.; Guðmundsson, A.; Bäckvall, J. E. Efficient aerobic oxidation of organic molecules by multistep electron transfer. *Angew. Chem. Int. Ed. Engl.* 2021, 60, 15686-704. DOI PubMed PMC
108. Klibanov, A. M. Asymmetric enzymatic oxidoreductions in organic solvents. *Curr. Opin. Biotechnol.* 2003, 14, 427-31. DOI PubMed
109. Yadav, M.; Joshi, C.; Paritosh, K.; et al. Organic waste conversion through anaerobic digestion: a critical insight into the metabolic pathways and microbial interactions. *Metab. Eng.* 2022, 69, 323-37. DOI
110. Caudillo-Flores, U.; Fuentes-Moyado, S.; Fernández-García, M.; Kubacka, A. Effect of niobium on the performance of Pd-TiO<sub>2</sub> photocatalysts for hydrogen production. *Catal. Today*. 2023, 419, 114147. DOI
111. Yan, Z.; Yin, K.; Xu, M.; et al. Photocatalysis for synergistic water remediation and H<sub>2</sub> production: a review. *Chem. Eng. J.* 2023, 472, 145066. DOI
112. Khatami, M.; Iravani, S. Green and eco-friendly synthesis of nanophotocatalysts: an overview. *Comments. Inorg. Chem.* 2021, 41, 133-87. DOI
113. Li, X.; Wang, L.; Fan, Y.; Feng, Q.; Cui, F.; Zhang, S. Biocompatibility and toxicity of nanoparticles and nanotubes. *J. Nanomater.* 2012, 2012, 548389. DOI
114. Saravanan, A.; Kumar, P. S.; Hemavathy, R. V.; et al. A review on synthesis methods and recent applications of nanomaterial in wastewater treatment: challenges and future perspectives. *Chemosphere* 2022, 307, 135713. DOI
115. Kalirajan, C.; Duple, A.; Nathanael, A. J.; Oh, T. H.; Manivasagam, G. A critical review on polymeric biomaterials for biomedical applications. *Polymers* 2021, 13, 3015. DOI PubMed PMC
116. Bokov, D.; Turki, J. A.; Chupradit, S.; et al. Nanomaterial by sol-gel method: synthesis and application. *Adv. Mater. Sci. Eng.* 2021, 2021, 5102014. DOI
117. Esposito, S. "Traditional" sol-gel chemistry as a powerful tool for the preparation of supported metal and metal oxide catalysts. *Materials* 2019, 12, 668. DOI PubMed PMC
118. Navas, D.; Fuentes, S.; Castro-Alvarez, A.; Chavez-Angel, E. Review on sol-gel synthesis of perovskite and oxide nanomaterials. *Gels* 2021, 7, 275. DOI PubMed PMC
119. Komarneni, S.; Roy, R.; Li, Q. Microwave-hydrothermal synthesis of ceramic powders. *Mater. Res. Bull.* 1992, 27, 1393-405. DOI
120. Hussain, M. K.; Khalid, N. Surfactant-assisted synthesis of MoO<sub>3</sub> nanorods and its application in photocatalytic degradation of different dyes in aqueous environment. *J. Mol. Liq.* 2022, 346, 117871. DOI
121. Fu, Q.; Cao, C.; Zhu, H. A solvothermal synthetic route to prepare polycrystalline carbon nitride. *Chem. Phys. Lett.* 1999, 314, 223-6. DOI
122. Walton, R. I. Subcritical solvothermal synthesis of condensed inorganic materials. *Chem. Soc. Rev.* 2002, 31, 230-8. DOI PubMed
123. Khater, G. A.; Nabawy, B. S.; El-Kheshen, A. A.; Abdel, L. M. A.; Farag, M. M. Use of arc furnace slag and ceramic sludge for the production of lightweight and highly porous ceramic materials. *Materials* 2022, 15, 1112. DOI PubMed PMC
124. Rahaman, M. N. Ceramic processing and sintering. 2nd edition. 2017: CRC press. DOI
125. Otitoju T, Ugochukwu Okoye P, Chen G, Li Y, Onyeka Okoye M, Li S. Advanced ceramic components: materials, fabrication, and applications. *J. Ind. Eng. Chem.* 2020, 85, 34-65. DOI
126. Schwarz, J. A.; Contescu, C.; Contescu, A. Methods for preparation of catalytic materials. *Chem. Rev.* 1995, 95, 477-510. DOI



127. Shukla, A.; Singh, S. C.; Bhardwaj, A.; et al. Calcination temperature induced structural, optical and magnetic transformations in titanium ferrite nanoparticles. *Reactions* **2022**, *3*, 224-32. DOI
128. Bogdanović, X.; Hinrichs, W. Influence of temperature during crystallization setup on precipitate formation and crystal shape of a metalloendopeptidase. *Acta. Crystallogr. Sect. F. Struct. Biol. Cryst. Commun.* **2011**, *67*, 421-3. DOI PubMed PMC
129. Theiss, F. L.; Ayoko, G. A.; Frost, R. L. Synthesis of layered double hydroxides containing  $Mg^{2+}$ ,  $Zn^{2+}$ ,  $Ca^{2+}$  and  $Al^{3+}$  layer cations by co-precipitation methods - a review. *Appl. Surf. Sci.* **2016**, *383*, 200-13. DOI
130. Dikshit, P.; Kumar, J.; Das, A.; et al. Green synthesis of metallic nanoparticles: applications and limitations. *Catalysts* **2021**, *11*, 902. DOI
131. Li, X.; Xu, H.; Chen, Z.; Chen, G. Biosynthesis of nanoparticles by microorganisms and their applications. *J. Nanomater.* **2011**, *2011*, 1-16. DOI
132. Dridi, S.; Bitri, N.; Mahjoubi, S.; Chaabouni, F.; Ly, I. One-step spray of  $Cu_2NiSnS_4$  thin films as absorber materials for photovoltaic applications. *J. Mater. Sci. Mater. Electron.* **2020**, *31*, 7193-9. DOI
133. Mazzotta, A.; Carlotti, M.; Mattoli, V. Conformable on-skin devices for thermo-electro-tactile stimulation: materials, design, and fabrication. *Mater. Adv.* **2021**, *2*, 1787-820. DOI
134. Iguchi, S.; Teramura, K.; Hosokawa, S.; Tanaka, T. A  $ZnTa_2O_6$  photocatalyst synthesized via solid state reaction for conversion of  $CO_2$  into CO in water. *Catal. Sci. Technol.* **2016**, *6*, 4978-85. DOI
135. Bouddouch, A.; Amaterz, E.; Bakiz, B.; et al. Phase transformation, photocatalytic and photoluminescent properties of  $BiPO_4$  catalysts prepared by solid-state reaction: degradation of rhodamine B. *Minerals* **2021**, *11*, 1007. DOI
136. Mazumdar, S. C.; Datta, S.; Alam, F. Structural, magnetic and transport properties of Gd and Cu Co-doped  $BiFeO_3$  multiferroics. *J. Appl. Mathemat. Phys.* **2022**, *10*, 2026-39. DOI
137. Zhao, W.; Luo, L.; Cong, M.; et al. Nanoscale covalent organic frameworks for enhanced photocatalytic hydrogen production. *Nat. Commun.* **2024**, *15*, 6482. DOI PubMed PMC
138. Khalid, N. R.; Arshad, A.; Tahir, M. B.; Hussain, M. K. Fabrication of p-n heterojunction  $Ag_2O@Ce_2O_3$  nanocomposites make enables to improve photocatalytic activity under visible light. *Appl. Nanosci.* **2021**, *11*, 199-206. DOI
139. Choudhary, R. K.; Kumaraswamy, G. N.; Baitha, R.; et al. Synthesis of  $BNiO_3$  nanocomposites for photocatalytic hydrogen production applications. *J. Inst. Eng. India. Ser. D.* **2024**. DOI
140. Thakur, A.; Manisha; Kumar, I.; Sharma, U. Visible light-induced functionalization of C-H bonds: opening of new avenues in organic synthesis. *Asian. J. Org. Chem.* **2022**, *11*, e202100804. DOI
141. Shang, F. K.; Qi, M. Y.; Tan, C. L.; Tang, Z. R.; Xu, Y. J. Nanoscale assembly of  $CdS/BiVO_4$  hybrids for coupling selective fine chemical synthesis and hydrogen production under visible light. *ACS. Phys. Chem. Au.* **2022**, *2*, 216-24. DOI PubMed PMC
142. Luo, J.; Wang, M.; Chen, L.; Shi, J. Efficient benzaldehyde photosynthesis coupling photocatalytic hydrogen evolution. *J. Energy. Chem.* **2022**, *66*, 52-60. DOI
143. Pang, Y.; Uddin, M. N.; Chen, W.; et al. Colloidal single-layer photocatalysts for methanol-storable solar  $H_2$  fuel. *Adv. Mater.* **2019**, *31*, e1905540. DOI
144. Liu, Z.; Yin, Z.; Cox, C.; et al. Room temperature stable  $CO_x$ -free  $H_2$  production from methanol with magnesium oxide nanophotocatalysts. *Sci. Adv.* **2016**, *2*, e1501425. DOI PubMed PMC
145. Cui, W.; Feng, L.; Xu, C.; Lü, S.; Qiu, F. Hydrogen production by photocatalytic decomposition of methanol gas on  $Pt/TiO_2$  nanofilm. *Catal. Commun.* **2004**, *5*, 533-6. DOI
146. Gazsi, A.; Schubert, G.; Bánsági, T.; Solymosi, F. Photocatalytic decompositions of methanol and ethanol on Au supported by pure or N-doped  $TiO_2$ . *J. Photoch. Photobio. A.* **2013**, *271*, 45-55. DOI
147. Uddin, N.; Langley, J.; Zhang, C.; et al. Zero-emission multivalORIZATION of light alcohols with self-separable pure  $H_2$  fuel. *Appl. Catal. B. Environ.* **2021**, *292*, 120212. DOI
148. Tan, H.; Kong, P.; Liu, M.; Gu, X.; Zheng, Z. Enhanced photocatalytic hydrogen production from aqueous-phase methanol reforming over cyano-carboxylic bifunctionally-modified carbon nitride. *Chem. Commun.* **2019**, *55*, 12503-6. DOI PubMed
149. Zhang, J.; Toe, C. Y.; Kumar, P.; Scott, J.; Amal, R. Engineering defects in  $TiO_2$  for the simultaneous production of hydrogen and organic products. *Appl. Catal. B. Environ.* **2023**, *333*, 122765. DOI
150. Tahir, M. Ni/MMT-promoted  $TiO_2$  nanocatalyst for dynamic photocatalytic  $H_2$  and hydrocarbons production from ethanol-water mixture under UV-light. *Int. J. Hydrogen. Energy.* **2017**, *42*, 28309-26. DOI
151. Zhang, X.; Luo, L.; Yun, R.; Pu, M.; Zhang, B.; Xiang, X. Increasing the activity and selectivity of  $TiO_2$ -supported Au catalysts for renewable hydrogen generation from ethanol photoreforming by engineering  $Ti^{3+}$  defects. *ACS. Sustainable. Chem. Eng.* **2019**, *7*, 13856-64. DOI
152. Li, P.; Yan, X.; Gao, S.; Cao, R. Boosting photocatalytic hydrogen production coupled with benzyl alcohol oxidation over  $CdS$ /metal-organic framework composites. *Chem. Eng. J.* **2021**, *421*, 129870. DOI
153. Jiang, D.; Chen, X.; Zhang, Z.; et al. Highly efficient simultaneous hydrogen evolution and benzaldehyde production using cadmium sulfide nanorods decorated with small cobalt nanoparticles under visible light. *J. Catal.* **2018**, *357*, 147-53. DOI
154. Tayyab, M.; Liu, Y.; Min, S.; et al. Simultaneous hydrogen production with the selective oxidation of benzyl alcohol to benzaldehyde by a noble-metal-free photocatalyst  $VC/CdS$  nanowires. *Chin. J. Catal.* **2022**, *43*, 1165-75. DOI
155. Zhang, Q.; Du, C.; Zhao, Q.; Zhou, C.; Yang, S. Visible light-driven the splitting of ethanol into hydrogen and acetaldehyde catalyzed by fibrous  $AgNPs/CdS$  hybrids at room temperature. *J. Taiwan. Inst. Chem. E.* **2019**, *102*, 182-9. DOI

156. Fu, X.; Leung, D. Y.; Wang, X.; Xue, W.; Fu, X. Photocatalytic reforming of ethanol to H<sub>2</sub> and CH<sub>4</sub> over ZnSn(OH)<sub>6</sub> nanocubes. *Int. J. Hydrogen. Energy*. **2011**, *36*, 1524-30. [DOI](#)
157. Liu, M.; Qiao, L.; Dong, B.; et al. Photocatalytic coproduction of H<sub>2</sub> and industrial chemical over MOF-derived direct Z-scheme heterostructure. *Appl. Catal. B. Environ.* **2020**, *273*, 119066. [DOI](#)
158. Zhang, F.; Li, J.; Wang, H.; et al. Realizing synergistic effect of electronic modulation and nanostructure engineering over graphitic carbon nitride for highly efficient visible-light H<sub>2</sub> production coupled with benzyl alcohol oxidation. *Appl. Catal. B. Environ.* **2020**, *269*, 118772. [DOI](#)
159. Lin, Q.; Li, Y.; Qi, M.; et al. Photoredox dual reaction for selective alcohol oxidation and hydrogen evolution over nickel surface-modified ZnIn<sub>2</sub>S<sub>4</sub>. *Appl. Catal. B. Environ.* **2020**, *271*, 118946. [DOI](#)
160. Hao, H.; Zhang, L.; Wang, W.; Qiao, S.; Liu, X. Photocatalytic hydrogen evolution coupled with efficient selective benzaldehyde production from benzyl alcohol aqueous solution over ZnS-Ni<sub>3</sub>S<sub>2</sub> composites. *ACS. Sustain. Chem. Eng.* **2019**, *7*, 10501-8. [DOI](#)

**Muhammad Khalid Hussain**

Muhammad Khalid Hussain received his Ph.D. in Material Science from the University of Gujrat (UOG), Pakistan, in 2023. He was awarded the IRSIP scholarship by the Australian National University (ANU), Australia, via HEC in 2022. From March 24, 2022, to September 18, 2023, he worked as a Lecturer of Physics at the UOG. He then joined ANU as a Post-Doctoral Research Fellow from September 21, 2023, to April 10, 2024. His research focuses on nanoscience and nanotechnology, particularly photocatalytic materials and the reaction engineering of photocatalytic processes. He has extensive hands-on experience with advanced microscopy (SEM) and spectroscopy techniques (UV-visible, PL, FTIR, XRD, and EDX), vacuum-based chemical vapor deposition (CVD) techniques using Argon gas and Gas Chromatography-Mass Spectrometry (GC-MS) for computing gas concentrations. He has published more than 22 research papers in well-reputed international journals with an impact factor of approximately 100.

**Ruhan Liu**

Ruhan Liu received his bachelor's degree from Shandong University, China, and the Australian National University, Australia, in 2023. He then completed his Master's degree at the Research School of Chemistry at the Australian National University (ANU). His current research focuses on photocatalytic reforming technology.



**Muhammad Tanveer**

Muhammad Tanveer graduated from Govt Zamindar College Gujrat, Pakistan, in 2003 and completed his MSc and M.Phil. degrees at the University of the Punjab Lahore, Pakistan, between 2005 and 2009. During his M.Phil. studies, he passed the PPSC exam and was selected as a lecturer at Govt. Abdul Haq College JPJ, Pakistan, where he served for two years. During this time, he was awarded a China Government Scholarship (CGS-2011) to pursue a PhD, which he completed in 2015 with 25 research publications. He was also honored with a distinguished Research Award by the Chinese government.

After completing his PhD, Dr. Tanveer served at Punjab University, Lahore, Pakistan, for one year (2015-2016) before joining the University of Lahore, Pakistan. At UOL, he served as the HOD of Physics at UOL Gujrat Campus for three years (2016-2019). On October 16, 2019, he joined the University of Gujrat (UOG), Pakistan, as an Assistant Professor on the Tenure Track System (TTS), where he has served for five years. He has recently been selected as the HOD of Physics at UOG Mandi Campus, Pakistan.

Dr. Tanveer has published more than 110 research manuscripts in well-reputed peer-reviewed journals, with an accumulated impact factor of 350. He has been recognized as one of the top 2% scientists globally in 2024, as listed by Stanford University and Elsevier.



**Khalid Nadeem Riaz  
(N. R. Khalid)**

Khalid Nadeem Riaz (N. R. Khalid) completed PhD in Physics, specializing in Material Physics, from Bahauddin Zakariya University, Multan, Pakistan, in 2014. During his PhD studies, he visited the Department of Material Science and Engineering, Zhejiang University, China, for six months under IRSIP, HEC scholarship.

Dr. Riaz worked as an Assistant Professor of Physics at the University of Gujrat, Gujrat, Pakistan, from April 1, 2015, to September 6, 2021. He then joined the University of Okara, Pakistan, on September 6, 2021, as an Associate Professor of Physics, where he continues to serve in this prestigious institution.

Dr. Riaz has published more than 189 international research papers, with an h-Index of 53 and approximately 7866 citations (source: Google Scholar). Additionally, he has edited seven book chapters in well-recognized books published by Springer and Elsevier. His book, "Photocatalysis and Nanomaterials in Chemistry: Mechanistic & Experimental Approaches", was recently published by Springer Nature.

Dr. Riaz has completed two SRGP research projects of HEC as PI and Co-PI. He also completed one NRPU, HEC project worth Rs. 4.57 million in 2020 at the University of Gujrat, Gujrat. Dr. Riaz received research productivity awards from the Pakistan Council of Science and Technology in 2013, 2014, 2015 and 2016.

**Zongyou Yin**

Professor Zongyou Yin obtained his B.S. and M.S. degrees at Jilin University in China and completed his Ph.D. at Nanyang Technological University (NTU) in Singapore. He then began his postdoctoral career at NTU/Singapore, followed by positions at IMRE/Singapore, MIT and Harvard University. Dr Yin established his research Group at the Australian National University (ANU) in 2017. His group's research is interdisciplinary, focusing on AI-driven innovations in materials, nano-to-atomic materials science, fundamental relationships among materials-structures-devices, and synergistic integration of multi-functions towards systems for energy and wearable applications. Dr. Yin is an Australian Research Council (ARC) Future Fellow, FRSC and FAIP.